

This is the final peer-reviewed accepted manuscript of:

Ortiz CJC, Silva M de F, Pruccoli L, Nadur NF, Azevedo LL de, Kümmerle AE, et al. Design, synthesis, and biological evaluation of new thalidomide–donepezil hybrids as neuroprotective agents targeting cholinesterases and neuroinflammation. RSC Med Chem. 25 May 2022;13(5):568–84.

The final published version is available online at: <https://dx.doi.org/10.1039/d1md00374g>

Terms of use:

Some rights reserved. The terms and conditions for the reuse of this version of the manuscript are specified in the publishing policy. For all terms of use and more information see the publisher's website.

This item was downloaded from IRIS Università di Bologna (<https://cris.unibo.it/>)

When citing, please refer to the published version.

ARTICLE

Design, synthesis, and biological evaluation of new thalidomide-donepezil hybrids as neuroprotective agents targeting cholinesterases and neuroinflammation

Received 00th January 20xx,
Accepted 00th January 20xx

DOI: 10.1039/x0xx00000x

Cindy Juliet Cristancho Ortiz^a, Matheus de Freitas Silva^a, Letizia Pruccoli^b, Nathália Fonseca Nadur^c, Luciana Luíza de Azevedo^c, Arthur Eugen Kümmerle^c, Isabella Alvim Guedes^d, Laurent Emmanuel Dardenne^d, Luiz Felipe Leomil Coelho^e, Marcos J. Guimarães^f, Fernanda M. R. da Silva^f, Newton Castro^f, Vanessa Silva Gontijo^a, Viviana C T Rojas^g, Merelym Ketterym de Oliveira^g, Fabiana Cardoso Vilela^g, Alexandre Giusti-Paiva^g, Gisele Barbosa^h, Lídia Moreira Lima^h, Gabriela Beserra Pinheiroⁱ, Leticia Germino Verasⁱ, Márcia Renata Mortariⁱ, Andrea Tarozzi^{ab} and Claudio Viegas Jr.^{*a}

A new series of eight multifunctional thalidomide-donepezil hybrids was synthesized based on the multi-target directed ligands strategy and evaluated as potential neuroprotective, cholinesterase inhibitors and anti-neuroinflammatory agents against neurodegenerative diseases. Molecular hybridization approach was used for structural design by combining the *N*-benzylpiperidine pharmacophore of donepezil and the isoindoline-1,3-dione fragment from thalidomide structure. The most promising compound PQM-189 (**3g**) showed good AChE inhibitory activity with IC₅₀ value of 3.15 μM, which was predicted by the docking studies as interacting with the enzyme in the same orientation observed in the AChE-donepezil complex and a similar profile of interaction. Additionally, compound **3g** significantly decreased in 43% and 39% iNOS and IL-1β levels, respectively, after 24h of incubation with lipopolysaccharide. In vivo data confirmed the ability of **3g** to prevent the locomotor impairment and changes in feeding behavior elicited by lipopolysaccharide. Moreover, PAMPA assay evidenced adequate blood-brain barrier and the gastrointestinal tract permeabilities with a Fa of 69.8%. Altogether, these biological data suggest that compound **3g** can treat the inflammatory process and oxidative stress resulting from the overexpression of iNOS and, therefore, the increase in reactive nitrogen species, and regulating the release of pro-inflammatory cytokines such as IL-1β. In this regard, compound PQM-189 (**3g**) revealed to be a promising neuroprotective and anti-neuroinflammatory agent with an innovative thalidomide-donepezil-based hybrid molecular architecture.

Introduction

Neuroinflammation has been implicated as a pathological hallmark in several neurodegenerative diseases (NDs), including Alzheimer's Disease (AD)¹, Parkinson's Disease (PD)², Huntington's Disease (HD)³ and multiple sclerosis⁴. NDs are

characterized by protein misfolding and accumulation of some specific protein aggregates inside the cell (tau or α-synuclein) or outside the cells (β-amyloid peptide (βA)), affecting different types of neurons and causing a set of signal processing impairment⁵. Under pathological conditions, toxic fragment protein deposits are accumulated in the brain and, in turn, activate immune cells, microglia and astrocytes through the release of pro-inflammatory mediators and toxins that further activate these cells, causing positive feedback, as well as neuronal and glial cell damage⁴. The disproportionate release of cytokines as well as reactive oxygen and nitrogen species (ROS and RNS) causes damage of healthy neurons, synaptic dysfunction, synapse loss, and neuronal death⁶. Therefore, an imbalance between pro-inflammatory and reparative functions of neuroimmune cells may result in a neuroinflammatory condition at central nervous system (CNS) level⁷.

It is not yet clear which is the triggering factor in NDs, however we know that ROS and RNS are likely to promote the disease progression through interaction with the mitochondria and therefore increase oxidative damage⁸. As a consequence, the

- PeQuiM-Laboratory of Research in Medicinal Chemistry, Federal University of Alfenas, 2600 Jovino Fernandes Sales Ave., Alfenas-MG 37130-840, Brazil
- Department for Life Quality Studies, University of Bologna'Alma Mater Studiorum', 237Corso d'Augusto St., 47921 Rimini, Italy
- Laboratory of Molecular Pharmacology, Institute of Biomedical Sciences, Federal University of Rio de Janeiro, 21941-902, Seropédica-RJ, Brazil
- National Laboratory for Scientific Computing, 25651-075, Petrópolis-RJ, Brazil
- Institute of Biomedical Sciences, Federal University of Alfenas, 700 Gabriel Monteiro da Silva St, Alfenas-MG 37130-840, Brazil
- Laboratory of Molecular Pharmacology, Institute of Biomedical Sciences, Federal University of Rio de Janeiro, 21941-902, Rio de Janeiro/RJ, Brazil
- Laboratory of Physiology, Federal University of Alfenas, 2600 Jovino Fernandes Sales Avenue, Alfenas-MG 37130-840, Brazil
- LASSBio - Laboratório de Avaliação e Síntese de Substâncias Bioativas, Health Sciences Center, Federal University of Rio de Janeiro, 21941-902, Rio de Janeiro/RJ, Brazil
- Laboratory of Neuropharmacology, Institute of Biological Sciences, University of Brasília, Brasília, DF 70910-900, Brazil

* E-mail address: cvviegas@gmail.com (C.Viegas Jr.) and andrea.tarozzi@unibo.it (A. Tarozzi)

abnormal increase of these species alter neuronal functions and activate inflammatory processes that lead to neurodegeneration⁹. Protection against external agents may occur through nitric oxide (NO) generation, after bacterial infection or other deleterious stimulation. In this process, inducible NO synthase (iNOS) generates NO by activating the immune response through the macrophage defense mechanism. However, overexpression of iNOS increases NO levels causing tissue damage, and high levels of NO is implicated in the pathophysiology of complex multifactorial diseases such as PD and AD. Data from literature indicate that selective inhibition of iNOS is an effective approach in the therapy of complex diseases by preventing the generation of RNS and treating inflammatory processes^{10,11}. Additionally, interleukin-1 β (IL-1 β), a pro-inflammatory cytokine, increases iNOS activity and stimulate NO production^{12,13}.

Recent studies have evidenced by cross communication between cholinergic signaling and brain immune cells in several neuroinflammatory diseases¹⁴. In particular, one of the possible mechanisms for controlling neuroinflammation is through the activation of the "cholinergic anti-inflammatory pathway" mediated by acetylcholine (ACh) binding to $\alpha 7$ nicotinic acetylcholinesterase receptor ($\alpha 7$ nAChR). According to these findings, acetylcholinesterase inhibitors (AChEIs) modulate innate immunity, probably by increasing the bioavailability of ACh in the synaptic cleft and activating the cholinergic anti-inflammatory pathway. As a result, AChEIs possess neuroprotective properties mediated by $\alpha 7$ nAChR, and this pathway represents a new option in pharmacological intervention in neurological disorders characterized by neuroinflammation¹⁵. Although the current clinically approved drugs act in the decrease and momentarily

slowdown the symptoms of complex NDs, they are not capable to interrupt or restore brain damage and disease progression. In the last years, considering the complex interconnection of multiple pathological factors related to the installation and progression of NDs, the design of multi-target directed ligands (MTDLs) has emerged as a hopeful strategy for the discovery of new disease modifying drugs. In general, this strategy is based on the molecular hybridization of different pharmacophore subunits from known biological active chemical entities, leading to novel molecular architectures that could simultaneously modulate multiple biological targets. The combination of multiple pharmacophores into a single molecule is a challenge, nevertheless it is expected that a single multi-target drug can bring benefits such as decreased metabolite formation and drug-drug interactions, with lower adverse side effects and an easier therapy management by needing fewer medications to effectively treat different disease symptoms¹⁶.

In terms of bioactivity, the isoindole fragment and its derivatives constitute an important class of biologically active heterocyclic compounds with a diversified pharmacological profile. This fragment is present in thalidomide (**2**), initially approved as a sedative for treating morning sickness in pregnant women, but it was banned in 1961 due to reports of teratogenicity. Thalidomide is currently successfully used to treat different chronic diseases, including leprosy, multiple myeloma, cancer, Crohn's disease and AIDS, but with severe restrictions and under FDA supervision¹⁷. However, thalidomide has also been shown to have therapeutic effects on NDs^{18,19} due to its ability to modulate several pro-inflammatory cytokines²⁰ and also to promote anti-apoptotic and antioxidant effect²¹.

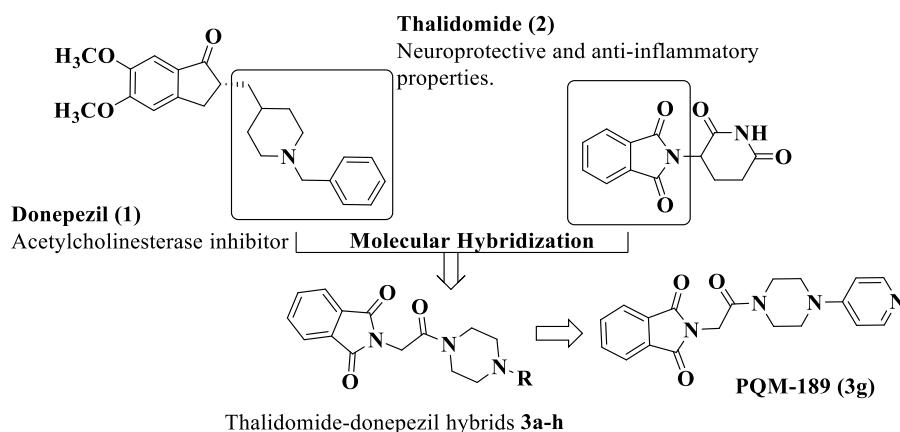


Figure 1. Design of a new series of multifunctional thalidomide-donepezil hybrids (**3a-h**).

Taking into account the anti-inflammatory effects of thalidomide (**2**), especially related to modulation of TNF- α , and the AChE inhibitory properties of donepezil (**1**), and based on the MTDL strategy, we designed a new series of potentially active multifunctional ligands (**3a-h**) by combining the *N*-

benzylpiperazine subunit as a bioisosteric fragment of the *N*-benzylpiperidine pharmacophore of donepezil and the isoindoline-1,3-dione fragment from thalidomide structure in a single scaffold (**Figure 1**). Moreover, the isoindoline-1,3-dione moiety, a pharmacophore for anti-inflammatory properties^{22,23},

was proposed to mimics the 2,3-dihydro-1*H*-indenone subunit present in donepezil and constitute a bioisosteric and second possible recognition subunit for cholinesterase inhibition. Herein, we describe the synthesis of this novel series of thalidomide-donepezil hybrids (**3a-h**) and the study of their anti-neuroinflammatory and anti-cholinesterase potential as neuroprotective drug candidates. We report the pharmacological evaluation of these compounds including the inhibition of cholinesterase activity, antioxidant properties and *in vitro* / *in vivo* anti-neuroinflammatory studies. In both *in vitro* and *in vivo* studies, we evaluated the ability of target-compounds to inhibit the inflammation induced by lipopolysaccharide (LPS), a component of the cell wall of gram-negative bacteria, that has been widely used to evoke the immune system in a rodent model, triggering an inflammatory process and mimic an infection response. After being recognized by the immune system, LPS activates an inflammatory cascade, releasing cytokines, which, upon reaching the CNS, will activate COX-2 and induce the synthesis of prostaglandins. In addition, it is possible to observe the activation of microglia and hypertrophy of astrocytes, establishing a picture of neuroinflammation²⁴.

Results and discussion

Synthesis

The synthesis of the target-compounds **3a-h** was based on the reaction of *N*-substituted piperazines **4a-h** with *N*-phthaloylglycine (**5**) in the presence of EDC, TEA and HOBT to provide the desired compounds **3a-h** in global yields of 60-70% (**Figure 2**). All compounds were characterized by IR, NMR and HRMS techniques.

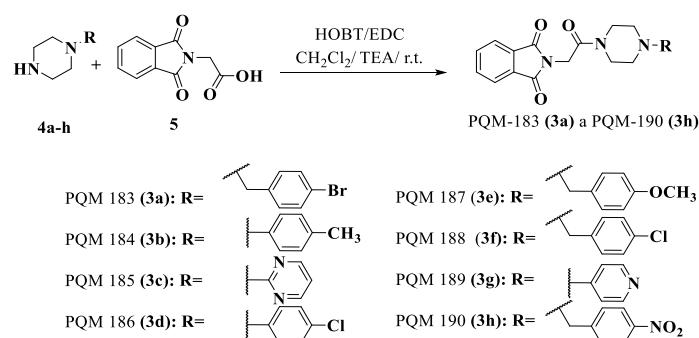


Figure 2. Synthetic route for the preparation of the thalidomide-donepezil hybrids **3a-h**

Table 1. Experimental data of *in vitro* inhibition of AChE and BuChE for compounds **3a-h**.

 PQM-183 to PQM-190 (3a-h)			
Compound	R	<i>ee</i> AChE % Inhibition	<i>eq</i> BuChE % Inhibition
PQM-183 (3a) ²⁵	4-bromobenzyl	8.38	-1.37
PQM-184 (3b)	<i>p</i> -tolyl	11.56	0.30
PQM-185 (3c)	pyrimidin-2-yl	39.65	-5.36
PQM-186 (3d) ²⁶	4-chlorophenyl	8.11	-2.09
PQM-187 (3e)	4-methoxybenzyl	17.13	25.36
PQM-188 (3f)	4-chlorobenzyl	7.82	1.26
PQM-189 (3g)	pyridin-4-yl	85.0 (IC ₅₀ = 3.15 ± 0.63)	-4.47
PQM-190 (3h)	4-nitrophenyl	16.93	-4.97

Activity values are indicated as IC₅₀.

Biological Results

In vitro AChE Inhibition

The inhibition of acetylcholinesterase (AChE) is the most widely used therapeutical approach in the treatment of AD and allows an increased level of ACh in the synaptic cleft. ACh is one of the main neurotransmitters responsible for physiology and functionality of CNS and is involved in both learning and memory processes. Currently, donepezil is considered the first-choice drug for AD treatment due to its efficacy in the selective inhibition of AChE activity, with no significant adverse effects, leading to significant cognitive and memory improvement. Thus, the modified Ellman's method²⁷ was used for screening the inhibitory

profile of the thalidomide-donepezil hybrids (**3a-h**) against both AChE and BuChE (butyrylcholinesterase) enzymes.

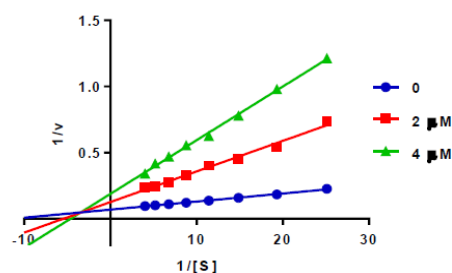


Figure 3. Lineweaver-Burk plots for AChE inhibition by PQM-189 (**3g**).

Preliminary results showed that only compound PQM-189 (**3g**) was capable to inhibit 85% of AChE activity at 30 μM , with all other compounds inhibiting AChE lower than 50% at the same concentration. Additionally, at the same concentration, no compounds significantly inhibited BuChE activity (Table 1), evidencing that compound **3g** acts as a selective AChE inhibitor, with an IC_{50} value of 3.15 μM . Kinetic studies (Figure 3) revealed

that **3g** was capable of binding both to the catalytic site (competitive inhibition) and to the allosteric site (non-competitive inhibition) of AChE, thereby acting in two different modes. Thus, experimental data evidenced that compound **3g** acts as a mixed type AChE inhibitor with $K_i = 0.72 \mu\text{M}$ and $K_i' = 1.68 \mu\text{M}$ (Table 2).

Table 2. Kinetic parameters of compound PQM-189 (**3g**) against AChE

Concentration (μM)	$V_{\text{max}} \pm \text{SD}^{\text{a}}$ ($\mu\text{M}/\text{min}$)	$K_{\text{m}} \pm \text{SD}^{\text{b}}$ (μM)	K_i (μM) $\pm \text{SD}^{\text{c}}$	K_i' (μM) $\pm \text{SD}^{\text{d}}$
0	16.37 ± 0.366	125.93 ± 4.92		
2	8.37 ± 0.428	156.00 ± 10.75	0.72 ± 0.007	1.68 ± 0.020
4	7.30 ± 0.215	253.70 ± 11.9		

a: Maximum velocity of the enzyme

b: Michaelis constant

c: competitive constant; d: non-competitive constant; data were shown in mean \pm SD of triplicate of independent experiments.

Molecular Docking Study with Human AChE

Considering the results from the *in vitro* AChE inhibition assay, molecular docking studies were performed with all target-compounds to predict their potential binding modes at the AChE binding cavity aiming to guide further optimizations of potential hits found. Due to the significant conformational changes observed in the peripheral anionic site (PAS), three representative conformations of AChE were selected, besides the structure of human AChE, complexed with donepezil (PDB code 4EY7): 1ZGC (*Torpedo californica*)²⁸, 2CKM (*Torpedo californica*)²⁹ and 1Q84 (*Mus musculus*)³⁰. In general, all compounds of this series exhibited more favorable docking score values against the 4EY7 conformation, which was expected, since they are structurally similar to donepezil.

The three compounds predicted to have the best binding affinities were PQM-188 (**3f**, XPGscore= -16.833) > PQM-183 (**3a**, XPGscore= -16.632) > PQM-189 (**3g**, XPGscore= -13.864), interacting with the AChE binding site in the same overall orientation (Figure 4), where the phthalimide moiety is located at the entrance of the gorge, while the phenyl group of the *N*-benzyl fragment interacts at the bottom of the cavity in a similar fashion of donepezil. In these three highlighted compounds, the phthalimide group interacts with Trp286 residue from the peripheral anionic site (PAS) through a π -stacking interaction and the carbonyl Oxygen makes a hydrogen bond with the Phe295 main chain (NH). In PQM-183 (**3g**) and PQM-188 (**3f**), the piperazine moiety interacts through cation- π interactions with the aromatic residues Trp86, Tyr337 and Phe338 (Figure 4A) – similarly to those observed for the piperidine group from

donepezil. Since PQM-183 (**3a**) and PQM-188 (**3f**) only differ in the halogen attached at the phenyl ring (*i.e.*, Br in PQM-183 (**3a**) and Cl in PQM-188 (**3f**)), they exhibit very similar binding modes and docking scores. The halogen atom of both **3a** and **3f** is located near to the Wat1, Ser203 and Glu202, but no halogen bonds were observed. Compound **3g** was the third compound with the best docking score (-13.864). The absence of a methylene group between the piperazine and the pyridine groups reduced the flexibility degree of this compound and, probably, affected the pKa of the Nitrogen atom of the pyridine ring, which was predicted as positively charged according to Epik software. Due to this protonation state, the cationic pyridine was able to perform a cation- π interaction with Trp86 residue at the bottom of the binding cavity (Figure 4B).

This important interaction is also observed on the AChE substrate and on a wide variety of potent AChE inhibitors^{31–33}. Finally, the docking results confirmed that PQM-189 (**3g**) is a dual inhibitor against AChE, showing an experimental conformation like that observed in the AChE-donepezil complex, and retaining the original orientation experimentally observed for donepezil. In addition, compound **3g** performs important interactions with Trp86, Phe295 and Trp286 residues. It is important to note that, according to our initial assumptions in planning the target series, the molecular docking study evidenced the importance of the *N*-benzylpiperazine and *N*-benzylpiperidine (from donepezil) subunits, that seem to operate as bioisosteric groups, to promote the necessary interactions at the CAS site, which according to the results from the *in vitro* assays, appear to be essential in the AChE inhibitory process.

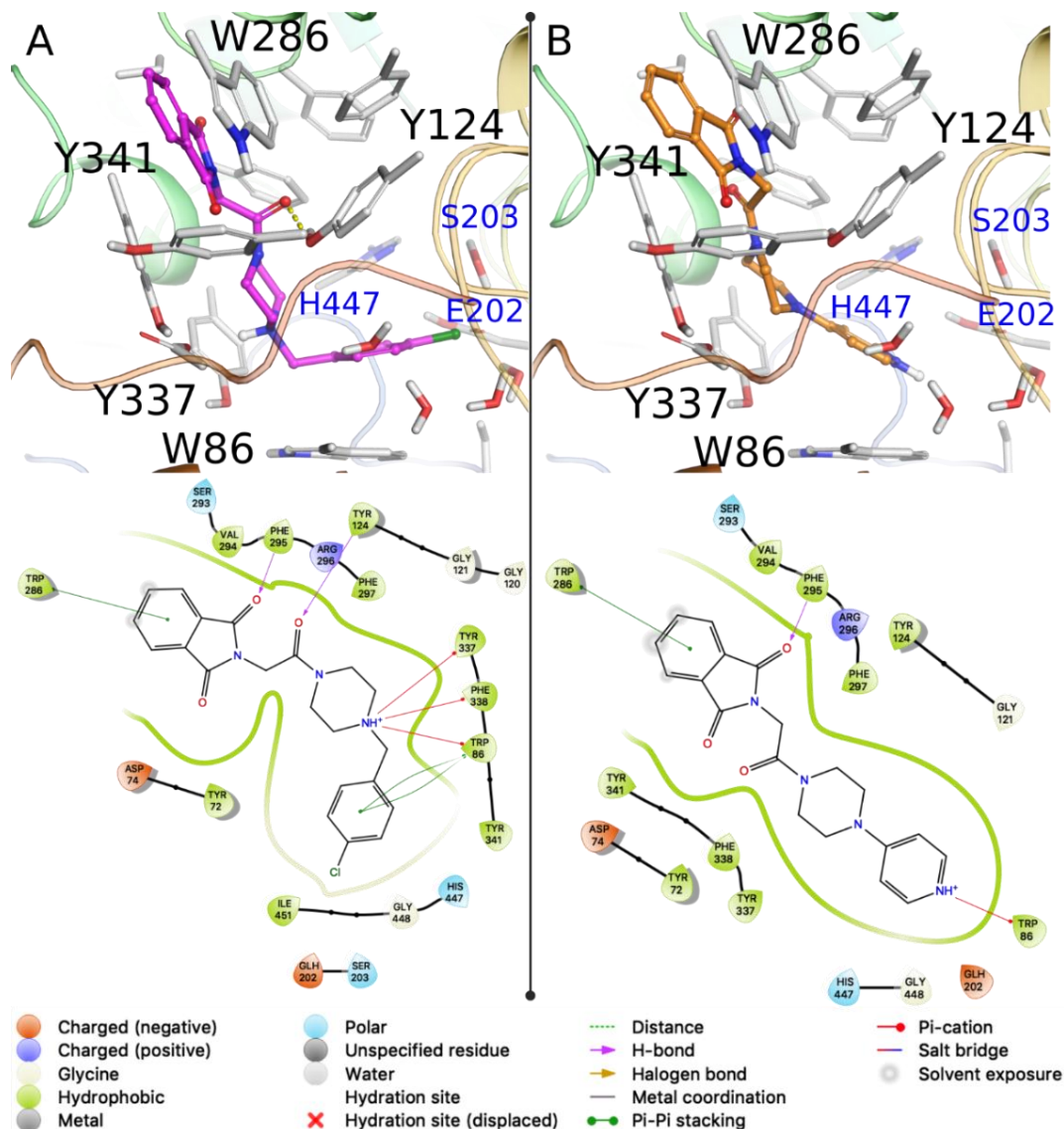


Figure 4. Predicted binding modes for PQM-188 (**3f**) (A) and PQM-189 (**3g**) (B) against the 4EY7 conformation of AChE. Residues making hydrogen bonds or stacking interactions with the ligand are labeled black. Other important residues are highlighted blue. Hydrogen bonds are represented as yellow dashes in the 3D picture. The Ligand Diagram Interaction is illustrated below the respective 3D image.

ADME Prediction *in silico*

In silico analysis was performed to predict the efficacy of the compounds against their molecular target and determine the ADME parameters (Absorption, Distribution, Metabolism and Excretion) that give an idea of the possible pharmacokinetics of the synthesized substances. Molecular structure is an important factor to predict the

pharmacokinetics profile of small molecules. Based on the molecular structure, we selected some ADME properties provided from QikProp (Schrödinger) module including lipophilicity, solubility, human oral absorption, and permeability. QikProp module from Schrödinger suite provides ranges for comparing a particular molecule property. The values of the observed properties are presented in **Table 3**.

ARTICLE

In silico ADME data

Table 3. *In silico* ADME data from QikProp v.3.5 software (Schrödinger) for the most active multitarget lead-compounds and donepezil

Compound	Molecular Volume ^a	QPlogPo/w ^b	QPlogS ^c	QPlogHERG ^d	QPlogBB ^e	QPlogKhsa ^f	QPPMDCK ^g	QPlogKp ^h	CNS ⁱ	% Human Oral Absorption ^j	Human Oral Absorption ^k
PQM 183	1229,953	2,12	-2,935	-5,602	-0,31	-0,443	240,718	-4,257	1	77,158	3
PQM 184	1174,164	2,41	-4,341	-4,782	-0,847	-0,253	311,285	-2,566	-1	88,877	3
PQM 185	1098,222	1,099	-2,858	-4,726	-1,036	-0,874	186,166	-2,893	-2	77,51	3
PQM 186	1158,1	2,588	-4,498	-4,783	-0,663	-0,299	767,407	-2,535	0	89,921	3
PQM 187	1253,102	1,603	-2,212	-5,572	-0,561	-0,619	90,962	-4,185	1	74,139	3
PQM 188	1220,948	2,04	-2,814	-5,573	-0,318	-0,469	223,94	-4,254	1	76,695	3
PQM 189	1101,684	1,077	-2,822	-4,66	-1,084	-0,864	160,269	-3,009	-2	76,299	3
PQM 190	1189,395	1,345	-3,818	-4,831	-1,937	-0,518	30,981	-4,275	-2	66,051	3
Donepezil	1266.695	4,368	-4,477	-6,608	0,189	0,569	485,175	-2,921		100	3
Values of reference*	500.0 – 2000.0	-2 - 6.5	-6.5 - 0.5	< -5 (not good)	-3 - 1.2	-1.5 - 1.5	<25 poor, > 500 great	-8.0 – -1.0	-2 - +2	<25% is Low	-1.5 – 1.5

*VR = gap or recommended value for 95% of known drugs (source: QikProp 3.2 Manual User – Schrödinger Software)

a: Total solvent-accessible volume in cubic angstroms using a probe with a 1.4 Å radius

b: Predicted octanol/water partition coefficient.

c: Predicted aqueous solubility, log S. S in mol dm⁻³ is the concentration of the solute in a saturated solution that is in equilibrium with the crystalline solid.

d: Predicted IC₅₀ value for blockage of HERG K⁺ channels.

e: Predicted brain/blood partition coefficient. Note: QikProp predictions are for orally delivered drugs so, for example, dopamine and serotonin are CNS negative because they are too polar to cross the blood-brain barrier

f: Prediction of binding to human serum albumin.

g: Predicted apparent MDCK cell permeability in nm/sec. MDCK cells are considered to be a good mimic for the blood-brain barrier. QikProp predictions are for non-active transport

h: Predicted skin permeability, log Kp.

i: Predicted central nervous system activity on a -2 (inactive) to +2 (active) scale.

j: Predicted human oral absorption on 0 to 100% scale.

k: Predicted qualitative human oral absorption: 1, 2, or 3 for low, medium, or high.

ARTICLE

Aqueous solubility Q_{logS} for our compounds were predicted to range from -2,21 to -4,49. Compounds with values less than -6 are poorly soluble. Lipophilicity was evaluated using the logarithm of the *n*-octanol/water partition coefficient $Q_{logPo/w}$. Partition coefficients are useful in the estimation of drug distribution within the organism³⁴. Higher lipophilicity makes it more likely to penetrate the BBB. A good permeability and solubility are to have a moderate Q_{logP} ($0 < \log P < 3$). For synthesized compounds, the predicted values of partition coefficients ranged from 1,07 to 2,58. However, the percentage of oral human absorption of our series lead compound **3g** was moderate, with a value of 76%. On the other hand, the ability to cross the blood-brain barrier (BBB) is expected to be one of the positive characteristics of the compounds to reach the CNS. BBB permeability values of our compounds were predicted to range from -0.31 to -1.91 and the compound **3g** is predicted to be inactive in CNS (-2) which indeed required for good drug candidature. Donepezil was included for comparison purposes (Table 3).

Cytotoxicity and antioxidant activity

Neurotoxicity was investigated in human neuroblastoma cells (SH-SY5Y cell line) by MTT assay. Compounds **3a-h** were assayed in eight different concentrations from 80 to 2.5 μM , in triplicate, and no significant cytotoxicity was observed at the maximum concentration. Although compounds **3c** and **3d** have the highest cytotoxicity of the series, the percentage of cell viability was greater than 50% toxicity. Considering the high dose of 80 μM , we can highlight that these data corroborate the safety of the compounds. Since the dose that they showed biological effect was in the range of 10 to 30 μM .

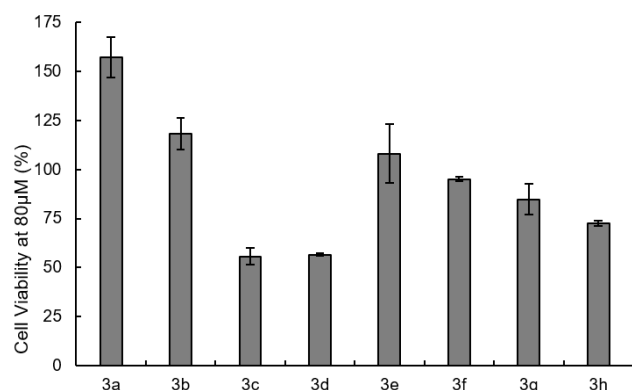


Figure 5. Percentage of cell viability at the maximum concentration (80 μM) by the MTT assay

The absence of cytotoxicity of the most active compound PQM-189 (**3g**) in AChE inhibition was also confirmed in VERO cell line, a

suitable model for studying the toxicity of new drug candidates^{35,36}. All compounds **3a-h** were additionally screened by potential antioxidant properties (radical scavenging capacity) in the DPPH assay at in different concentrations (1.56-200 μM). Each target compounds were added to a DPPH (2,2-diphenyl-1-picrylhydrazyl) solution and, after a 30 min period, the absorbance was recorded. However, none of the thalidomide-donepezil hybrids showed antioxidant activity, probably due to the absence of favorable structural characteristics to apply radical scavenging ability.

Parallel artificial membrane permeability assay (PAMPA)

The permeability profile through the gastrointestinal tract (GIT) and blood-brain barrier (BBB) of the target-compounds was evaluated using the parallel artificial membrane permeability (PAMPA) test^{37,38}. The permeability result for PAMPA-GIT classifies the compounds according to the percentage of absorbed fraction (Fa%), as: high intestinal permeability (70-100%), medium permeability (30-69%) or low permeability (0-29%)³⁹. The PAMPA-BBB model classifies the compounds only as: permeable (BBB+) or non-permeable (BBB-)^{38,40}. The permeability result for PAMPA-GIT classifies the compounds according to the percentage of absorbed fraction (Fa%) as: high intestinal permeability (70-100%), medium permeability (30-69%) or low permeability (0-29%). The PAMPA-BBB model classifies the compounds only as: permeable (CNS+) or non-permeable (CNS-).

Compound **3g** displayed high permeability through BBB, determined by PAMPA-BBB test (P_e 13.89 $\times 10^{-6}$ $\text{cm}\cdot\text{s}^{-1}$), being considered CNS+ ($P_e > 4.0$). In addition, this compound showed moderate permeability across GIT, with P_e 3.15 $\times 10^{-6}$ $\text{cm}\cdot\text{s}^{-1}$ and Fa 69.8%. Although *in silico* prediction predicted that our lead compound **3g** was inactive in the CNS. The permeability test indicated a positive response demonstrating that *in silico* studies must be confirmed and are only a guide to know and understand the potential of new compounds. All data are available in supplementary data.

In vitro Anti-inflammatory Activity and Neuronal Plasticity

The gene expression of iNOS and pro-inflammatory cytokines, including IL-1 β and COX-2, was evaluated in microglial THP-1 cells, after 24 h of treatment with LPS (1 $\mu\text{g}/\text{mL}$) in the presence of PQM-189 (**3g**, 10 μM) by RT-PCR. As disclosed in figure 6, compound **3g** significantly decreased iNOS and IL-1 β level with 43% and 39% of inhibition, respectively, with no significant effect on COX-2 expression.

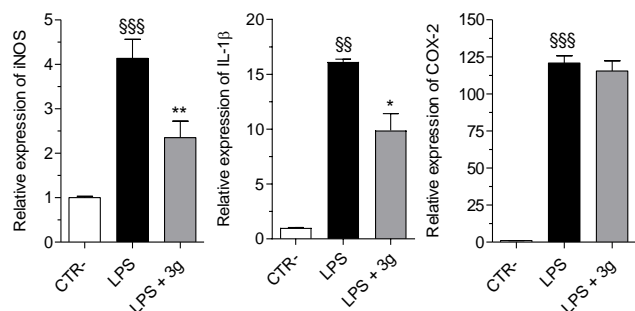


Figure 6. In vitro anti-inflammatory activity of compound **3g** against LPS-induced inflammation in microglial THP-1 cells. Cells were incubated for 24 h with compound **3g** (10 μ M) and LPS (1 μ g/mL). At the end of incubation, iNOS, IL-1 β and COX-2 expression was measured by quantitative RT-PCR. Data are reported as mean \pm SEM of three independent experiments (SSS p <0.001 and SS p <0.01 vs untreated cells; ** p <0.01 and * p <0.05 vs cells treated with LPS at one-way ANOVA with Bonferroni post hoc test).

In parallel, we evaluated the ability of **3g** to promote neuronal plasticity in terms of synaptophysin (SYP) and brain-derived neurotrophic factor (BDNF) gene expression in neuroblastoma SH-SY5Y cells after differentiation to mature neuron-like phenotype. As a result, compound **3g** significantly promoted the expression of SYP, but not BDNF, in differentiated SH-SY5Y cells (**Figure 7**).

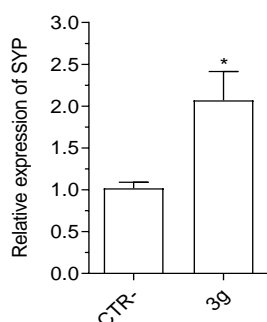


Figure 7. Effect of compound **3g** on SYP gene expression in differentiated SH-SY5Y cells. Cells were incubated for 24 h with 10 μ M PQM-189 (**3g**). At the end of incubation, SYP expression was measured by quantitative RT-PCR. Data are reported as mean \pm SEM of three independent experiments (* p <0.05 vs untreated cells with Student's *t*-test).

In vitro activity against A β -aggregates

In order to complete the investigation of PQM-189 (**3g**), its possible ability on disaggregation of A β ₁₋₄₂ with fluorescent detection of thioflavin was assessed. In the A β ₁₋₄₂ disaggregation test, the ThT fluorescence was able to identify **3g** and A β ₁₋₄₂ control (treatment: $F_{(2,19)} = 62.12$, $p < 0.0001$; time: $F_{(4,76)} = 11.74$, $p < 0.0001$ and interaction $F_{(8,76)} = 3.275$, $p = .0029$). The two-way ANOVA test with Bonferroni post-hoc test showed no significant

difference when compared to the test compound **3g** and A β ₁₋₄₂ control. Moreover, regarding the endpoint, compound **3g** did not show a disaggregating effect of A β ₁₋₄₂ comparing the H₂O group, A β ₁₋₄₂ group and the effect of PQM-189 (**3g**) ($F_{(2,19)} = 72.19$, $p < 0.0001$).

In vivo Feeding and Open Field Behavior

To evaluate the effect of compound **3g** against an inflammatory-like condition, a group of adult male Wistar rats received an intraperitoneal administration of lipopolysaccharide (LPS). As shown in **Figure 8**, after a 24 hr period, we observed a significant reduction in food intake in the vehicle + LPS group ($p < 0.001$), when compared to the vehicle + saline group. However, pre-treatment with compound **3g** was able to prevent that reduction in feeding behavior induced by LPS, that is, there was an increase in food intake in adult male Wistar rats in the **3g** + LPS group ($p < 0.01$), when compared to vehicle + LPS group (LPS factor: $F_{(3,96)} = 183.60$, $p < 0.001$; **3g** factor: $F_{(3,96)} = 18.04$, $p < 0.001$; LPS + **3g** factor: $F_{(9,96)} = 6.42$, $p < 0.001$). This result not only shows that compound **3g** does not negatively influence adult male rats behavior, but quite the opposite, evidence that it was able to counteract the LPS-induced inflammatory symptoms, since loss of appetite is a common sickness behavior.

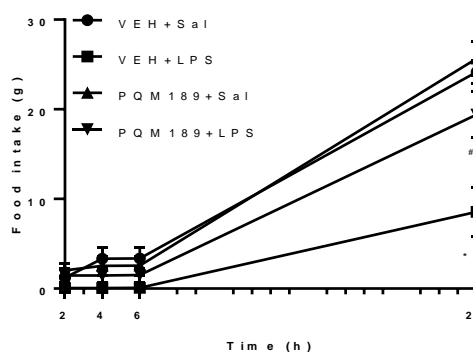


Figure 8. Food intake 2, 4, 6 and 24 hr after application of LPS, in adult male Wistar rats that received pretreatment with vehicle or PQM-189 (**3g**). *** p <0.001 when compared to VEH + Sal group; ## p <0.01 when compared to VEH + LPS group. VEH: vehicle; Sal: Saline.

Open Field Behavioral Test

Sickness-like behavior induced by LPS was measured by locomotory activity in the open field test. LPS administration a general evaluate the autonomous behavior, curiosity, inquiry behavior in new environments. The total distance traveled, and number of standing events are used to assess locomotor activity. In this behavioral test, as depicted in **Figure 9**, we observed that after 2 hr of LPS administration, the adult male Wistar rats showed an increase in immobility time ($p < 0.001$), when compared to the control (VEH + saline group). Meanwhile, pre-treatment with PQM-189 (**3g**) significantly prevented the reduction in traveled distance and led to a decrease in immobility

time induced by LPS, since there was no difference between the groups **3g** + LPS when compared to VEH + saline (A: LPS factor: $F_{(1,23)} = 26.64$, $p < 0.001$; **3g** factor: $F_{(1,23)} = 3.54$, $p > 0.05$; LPS + **3g** factor: $F_{(1,23)} = 3.52$, $p > 0.05$; B: LPS factor: $F_{(1,23)} = 22.82$, $p < 0.001$; **3g** factor: $F_{(1,23)} = 2.07$, $p > 0.05$; LPS + **3g** factor: $F_{(1,23)} = 4.07$, $p > 0.05$).

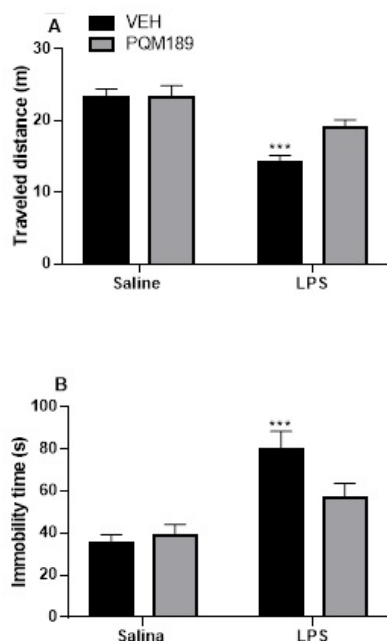


Figure 9. Effect of pretreatment with PQM-189 (**3g**) on LPS-induced neuroinflammation in the open field test A – traveled distance in meters (m) and in B – immobility time in seconds (s). *** $p < 0.001$ when compared to VEH + saline. VEH: vehicle.

Discussion

Nowadays, it is very well documented in the literature that neuroinflammation is a central player in the onset, progress e severity of major NDs, such as AD and PD. Moreover, a complex network of interconnected events such as protein deposition (e.g. A β and tau in AD, α -synuclein in PD), OS, activation of microglia, astrocyte and immune system could contribute decisively to the installation and progress of the inflammation process into CNS^{41–46}.

On the other hand, it is well described that free LPS in bloodstream binds to lipopolysaccharide binding protein (LBP) to form LBP-LPS complex, which activates different inflammatory-related cell populations (monocyte, neutrophils, and macrophages) by binding to its CD14 and TLR4 receptors. Thus, one of the clearest consequences of this activation is the production of pro-inflammatory cytokines (TNF- α , IL-1 and IL-6), which act on the CNS and activate COX-2 and prostaglandin E synthase, which, in turn, stimulate the synthesis of PGE2⁴⁷. Once concentration of PGE2 is increased, it promotes activation of the HPA axis and neurons in the preoptic area, leading to the development of the febrile response^{48–50}.

Norden et al.⁵¹ reported that the activation of the immune system by LPS is also capable of inducing a coordinated response in the CNS, which could interpret and propagate inflammatory signals in the brain and, in turn, affect physiological and behavioral events. In response to these changes at the immunological and endocrine levels and in the glial face of an inflammatory-infectious stimulus, it was observed behavioral and thermoregulatory changes in adult male Wistar rat models. Emphasizing the behavioral parameter, studies have shown that LPS induced behavioral impairments including increased immobile time, low curiosity, and lack of appetite^{52,53}. In this regard, more recent studies also report that the inflammation elicited by LPS can affect both the cholinergic activity and the neuronal plasticity, similarly to the observed changes in AD, suggesting an interaction among different players on behavior and neuroinflammatory response^{54–56}.

Among the all-tested thalidomide-donepezil hybrids, PQM-189 (**3g**) showed the most significantly ability to inhibit both the AChE activity and neuroinflammation in *in vitro* models, but no significant effect was observed on disaggregation of A β . Interestingly, **3g** also recorded the property to stimulate the gene expression of SYP, suggesting its ability to prevent the impairment of synaptic plasticity evoked by inflammatory and neurodegenerative processes. In this regard, PQM-189 (**3g**) may retain some of the neuroprotective effects of donepezil, as expected. In fact, recent studies have shown the contribution of donepezil to facilitate the recovery of synaptic protein impairment in different animal models^{57,58}.

In addition, our *in vivo* studies confirmed the ability of PQM-189 (**3g**) to prevent the impairment of locomotor activity and feeding behavior elicited by LPS. Adult male Wistar rats that received LPS showed a reduction in the traveled distance and an increase in immobility time in the open field model. In contrast, pre-treatment with **3g** was able to prevent these effects induced by endotoxin. When evaluated the feeding behavior, it was noticed a decrease in food intake, 24 hr after the administration of LPS. However, when adult male Wistar rats were treated with PQM-189 (**3g**) previously to LPS administration, the food intake was increased when compared to the VEH + LPS group. These findings allow us to suggest that the treatment with PQM-189 (**3g**), before the administration of LPS, can prevent the behavioral changes induced by endotoxin, regarding locomotor activity and feeding behavior, through its ability to target the cholinergic system, in addition to neuroinflammation and synaptic dysfunction.

Finally, although the *in silico* ADME parameters results did not indicate a positive relationship for compound **3g** to cross the BBB and reach the CNS, the PAMPA permeability assays showed that our compound **3g** displayed high permeability through BBB, being considered CNS+ and showed moderate permeability across GIT.

EXPERIMENTAL SECTION

Chemistry

The Infrared (IR) spectra have been generated in an infrared spectrometer Thermo Scientific USA (Nicolet i550 model) coupled to Pike Gladi ATR technologies in analysis and characterization of drugs laboratory (LACFar) at Federal University of Alfenas (UNIFAL-MG). Nuclear Magnetic Resonance (NMR) spectra of ^1H and ^{13}C were obtained on a Bruker AC-300 spectrometer operating at 300 MHz for ^1H NMR and 75 MHz for ^{13}C NMR. The samples were solubilized in chloroform deuterated using tetramethylsilane as the internal reference. Mass spectrometric analyzes were acquired in a range of m/z of 80-1000 in the BRUKER COMPASS mass spectrometer by electrospray ionization. The purity of compounds was determined by High Performance Liquid Chromatography (HPLC). Thin layer chromatography experiments were performed on silica gel sheet 60 F254, Merck and purification by chromatography column was performed on flash silica gel (220–440 mesh, 0.035mm–0.075 mm), Sigma-Aldrich. The visualization of the substances was done in UV chamber ($\lambda=254$ or 365 nm). Melting point was made on a Mars equipment (PFM II) with crushed sample and packaged in capillary tube. All spectra are available in the supplementary material.

Synthesis of Thalidomide-Donepezil Hybrids 3a-h

Compounds **3a-h** were obtained according to methodology of Anil K Singh and co-workers⁵⁹. To a solution of *N*-phthaloylglycine (2.5 mmol) in dichloromethane (15 mL), *N*-(3-Dimethylaminopropyl)-*N'*-ethylcarbodiimide hydrochloride (EDC-HCl, 2.5 mmol) and triethylamine (TEA, 5.1 mmol) were added, and reaction mixture was stirred at 0°C for 15 min. Then, hydroxybenzotriazole (HOBT, 2.5 mmol) was added and the reaction mixture was stirred for additional 15 min at 0°C. After this initial period of 30 min commercially available *N*-substituted piperazines (**5a-h**) were added and the reaction mixture was stirred for another 24 h at room temperature. Then, the solvent was removed, and the resultant crude product was extracted with ethyl acetate, washed with water, dried with anhydrous MgSO_4 and filtered. The organic layer was concentrated under reduced pressure to give the desired products, which were purified by flash column chromatography using dichloromethane-methanol (9.5:0.5) as eluent or filtered and recrystallized from ethyl acetate or mixture of ethyl acetate/hexane (7:3) to give the desired pure products **3a-h**. All compounds were characterized by IR, ^1H and ^{13}C NMR techniques and HRMS. All spectra are available in supporting information (Figure. 1 – Figure. 40).

2-(2-(4-(4-bromobenzyl)piperazin-1-yl)-2-oxoethyl)isoindoline-1,3-dione **PQM-183 (3a)**. Yellow light solid (yield 32%), m.p. 156°C. IR (ATR): ν 2938, 2915, 1776, 1711 and 1667 cm^{-1} . ^1H NMR (300 MHz, CDCl_3) δ 7.86 (dd, $J = 3.0$ and 5.6 Hz, 2H, Ar-H), 7.71 (dd, $J = 3.0$ and 5.6 Hz, 2H, Ar-H), 7.45 (d, $J = 8.4$ Hz, 2H, Ar-H), 7.21 (d, $J = 8.4$ Hz, 2H, Ar-H), 4.48 (s, 2H, CH_2CO), 3.61 (t, 2H, $\text{NCH}_2\text{CH}_2\text{N}$), 3.52 (t, 2H, $\text{NCH}_2\text{CH}_2\text{N}$), 3.48 (s, 2H, CH_2), 2.50 (t, 2H, $\text{NCH}_2\text{CH}_2\text{N}$), 2.43 (t, 2H, $\text{NCH}_2\text{CH}_2\text{N}$). ^{13}C NMR (75 MHz, CDCl_3) δ 168.1, 163.9, 136.7, 134.1,

132.3, 131.5, 130.9, 123.5, 121.2, 62.1, 52.5, 52.2, 44.8, 42.3 and 39.1. HR-MS (ESI) m/z : Calcd for $\text{C}_{21}\text{H}_{20}\text{BrN}_3\text{O}_3$ $[\text{M}+\text{H}]^+$: 442.0766, found: 442.0758.

*2-(2-oxo-2-(4-(*p*-tolyl)piperazin-1-yl)ethyl)isoindoline-1,3-dione* **PQM-184 (3b)**. Yellow light solid (yield 55%), m.p. 192°C. IR (ATR): ν 2989, 2908, 1778, 1706, 1638 and 1513 cm^{-1} . ^1H NMR (300 MHz, CDCl_3) δ 7.88 (dd, $J = 3.0$ and 5.5 Hz, 2H, Ar-H), 7.72 (dd, $J = 3.0$ and 5.5 Hz, 2H, Ar-H), 7.10 (d, $J = 8.1$ Hz, 2H, Ar-H), 6.86 (d, $J = 8.1$ Hz, 2H, Ar-H), 4.54 (s, 2H, CH_2CO), 3.76 (t, 2H, $\text{NCH}_2\text{CH}_2\text{N}$), 3.69 (t, 2H, $\text{NCH}_2\text{CH}_2\text{N}$), 3.22 (t, 2H, $\text{NCH}_2\text{CH}_2\text{N}$), 3.12 (t, 2H, $\text{NCH}_2\text{CH}_2\text{N}$), 2.28 (s, 3H, CH_3). ^{13}C NMR (75 MHz, CDCl_3) δ 168.1, 164.0, 148.8, 134.1, 132.3, 130.4, 129.8, 123.6, 117.2, 50.1, 49.9, 44.8, 42.3, 39.1 and 20.5. HR-MS (ESI) m/z : Calcd for $\text{C}_{21}\text{H}_{21}\text{N}_3\text{O}_3$ $[\text{M}+\text{H}]^+$: 364.1661, found: 364.1641.

2-(2-oxo-2-(4-(pyrimidin-2-yl)piperazin-1-yl)ethyl)isoindoline-1,3-dione **PQM-185 (3c)**. White solid (yield 70%), m.p. 258°C. IR (ATR): 2990, 2808, 1778, 1704, 1637 and 1515 cm^{-1} . ^1H NMR (300 MHz, CDCl_3) δ 8.33 (d, $J = 4.7$ Hz, 2H, Ar-H), 7.87 (dd, $J = 3.1$ and 5.4 Hz, 2H, Ar-H), 7.72 (dd, $J = 3.1$ and 5.4 Hz, 2H, Ar-H), 6.55 (t, 2H, Ar-H), 4.55 (s, 2H, CH_2CO), 3.97 (t, 2H, $\text{NCH}_2\text{CH}_2\text{N}$), 3.86 (t, 2H, $\text{NCH}_2\text{CH}_2\text{N}$), 3.69 (t, 2H, $\text{NCH}_2\text{CH}_2\text{N}$), 3.61 (t, 2H, $\text{NCH}_2\text{CH}_2\text{N}$). ^{13}C NMR (75 MHz, CDCl_3) δ 168.0, 164.3, 161.5, 157.8, 134.1, 132.3, 123.6, 110.6, 44.6, 43.4, 42.1 and 39.2. HR-MS (ESI) m/z : Calcd. for $\text{C}_{18}\text{H}_{17}\text{N}_5\text{O}_3$ $[\text{M}+\text{Na}]^+$: 374.1229, found: 374.1209.

2-(2-(4-(4-chlorophenyl)piperazin-1-yl)-2-oxoethyl)isoindoline-1,3-dione **PQM-186 (3d)**. White solid (yield 36%), m.p. 230°C. IR (ATR): ν 2989, 2813, 1778, 1704 and 1639 cm^{-1} . ^1H NMR (300 MHz, CDCl_3) δ 7.87 (dd, $J = 3.0$ and 5.5 Hz, 2H, Ar-H), 7.72 (dd, $J = 3.0$ and 5.5 Hz, 2H, Ar-H), 7.23 (d, $J = 9.1$ Hz, 2H, Ar-H), 6.85 (d, $J = 9.1$ Hz, 2H, Ar-H), 4.53 (s, 2H, CH_2CO), 3.75 (t, 2H, $\text{NCH}_2\text{CH}_2\text{N}$), 3.69 (t, 2H, $\text{NCH}_2\text{CH}_2\text{N}$), 3.24 (t, 2H, $\text{NCH}_2\text{CH}_2\text{N}$), 3.14 (t, 2H, $\text{NCH}_2\text{CH}_2\text{N}$). ^{13}C NMR (75 MHz, CDCl_3) δ 168.0, 164.0, 149.4, 134.1, 132.3, 129.2, 125.7, 123.6, 118.0, 49.5, 49.3, 44.6, 42.1 and 39.1. HR-MS (ESI) m/z : Calcd for $\text{C}_{20}\text{H}_{18}\text{ClN}_3\text{O}_3$ $[\text{M}+\text{Na}]^+$: 406.0934 found: 406.0915.

2-(2-(4-(4-methoxybenzyl)piperazin-1-yl)-2-oxoethyl)isoindoline-1,3-dione **PQM-187 (3e)**. White solid (yield 41%), m.p. 166°C. IR (ATR): ν 2928, 2831, 1772, 1709, 1656 and 1513 cm^{-1} . ^1H NMR (300 MHz, CDCl_3) δ 7.86 (dd, $J = 3.1$ and 5.4 Hz, 2H, Ar-H), 7.71 (dd, $J = 3.1$ and 5.4 Hz, 2H, Ar-H), 7.23 (d, $J = 8.7$ Hz, 2H, Ar-H), 6.86 (d, $J = 8.7$ Hz, 2H, Ar-H), 4.47 (s, 2H, CH_2CO), 3.80 (s, 3H, OCH_3), 3.60 (t, 2H, $\text{NCH}_2\text{CH}_2\text{N}$), 3.52 (t, 2H, $\text{NCH}_2\text{CH}_2\text{N}$), 3.48 (s, 2H, CH_2), 2.50 (s, 2H, CH_2), 2.43 (t, 2H, $\text{NCH}_2\text{CH}_2\text{N}$). ^{13}C NMR (75 MHz, CDCl_3) δ 168.1, 163.8, 158.9, 134.0, 132.3, 130.3, 129.5, 123.5, 113.7, 62.2, 55.3, 52.6, 52.4, 44.8, 42.3 and 39.1. HR-MS (ESI) m/z : Calcd for $\text{C}_{22}\text{H}_{23}\text{N}_3\text{O}_4$ $[\text{M}+\text{H}]^+$: 394.1759, found: 394.1759.

2-(2-(4-(4-chlorobenzyl)piperazin-1-yl)-2-oxoethyl)isoindoline-1,3-dione **PQM-188 (3f)**. White solid (yield 27%), m.p. 146°C. IR (ATR): ν 2940, 2816, 1776, 1712 and 1688 cm^{-1} . ^1H NMR (300 MHz, CDCl_3) δ 7.86 (dd, $J = 3.0$ and 5.4 Hz, 2H, Ar-H), 7.71 (dd, $J = 3.0$ and 5.4 Hz, 2H, Ar-H), 7.36-7.12 (m, 4H, Ar-H), 4.47 (s, 2H, CH_2CO), 3.60 (t, 2H,

$\text{NCH}_2\text{CH}_2\text{N}$), 3.52 (t, 2H, $\text{NCH}_2\text{CH}_2\text{N}$), 3.50 (s, 2H, CH_2), 2.50 (t, 2H, $\text{NCH}_2\text{CH}_2\text{N}$), 2.43 (t, 2H, $\text{NCH}_2\text{CH}_2\text{N}$). ^{13}C NMR (75 MHz, CDCl_3) δ 168.1, 163.9, 136.2, 134.1, 133.1, 132.3, 130.3, 128.5, 123.5, 62.0, 52.7, 52.5, 44.8, 42.3 and 39.1. HR-MS (ESI) m/z : Calcd for $\text{C}_{21}\text{H}_{20}\text{ClN}_3\text{O}_3$ $[\text{M}+\text{H}]^+$: 398.1271, found: 398.1271.

2-(2-oxo-2-(4-(pyridin-4-yl)piperazin-1-yl)ethyl)isoindoline-1,3-dione **PQM-189 (3g)**. White solid (yield 32%), m.p. 238°C. IR (ATR): ν 2897, 2857, 1769, 1716, 1651 and 1512 cm^{-1} . ^1H NMR (300 MHz, CDCl_3) δ 8.31 (d, $J = 5.6$ Hz, 2H, Ar-H), 7.87 (dd, $J = 3.0$ and 5.2 Hz, 2H, Ar-H), 7.72 (dd, $J = 3.0$ and 5.2 Hz, 2H, Ar-H), 6.66 (d, $J = 5.6$ Hz, 2H, Ar-H), 4.53 (s, 2H, CH_2CO), 3.82-3.62 (m, 4H, $\text{NCH}_2\text{CH}_2\text{N}$), 3.49 (t, 2H, $\text{NCH}_2\text{CH}_2\text{N}$), 3.39 (t, 2H, $\text{NCH}_2\text{CH}_2\text{N}$). ^{13}C NMR (75 MHz, CDCl_3) δ 168.0, 164.3, 154.5, 150.3, 134.2, 132.2, 123.6, 108.6, 45.7, 44.1, 41.5 and 39.0. HR-MS (ESI) m/z : Calcd for $\text{C}_{19}\text{H}_{18}\text{N}_4\text{O}_3$ $[\text{M}+\text{H}]^+$: 351.1457, found: 351.1343.

2-(2-(4-(4-nitrophenyl)piperazin-1-yl)-2-oxoethyl)isoindoline-1,3-dione **PQM-190 (3h)**. Yellow solid (yield 28%), m.p. >300°C. IR (ATR): ν 2973, 2956, 1775, 1712, 1651 and 1589 cm^{-1} . ^1H NMR (300 MHz, CDCl_3) δ 8.07 (d, $J = 9.5$ Hz, 2H, Ar-H), 7.85-7.93 (m, 4H, Ar-H), 7.02 (d, $J = 9.5$ Hz, 2H, Ar-H), 4.59 (s, 2H, CH_2CO), 3.75 (dd, $J = 4.1$ and 6.5 Hz, 2H, $\text{NCH}_2\text{CH}_2\text{N}$), 3.60-3.57 (m, 4H, $\text{NCH}_2\text{CH}_2\text{N}$), 3.51 (dd, $J = 3.8$ and 7.5 Hz, 2H, $\text{NCH}_2\text{CH}_2\text{N}$). ^{13}C NMR (75 MHz, CDCl_3) δ 168.1, 165.0, 154.8, 137.5, 135.2, 132.1, 126.2, 123.8, 113.1, 46.4, 46.1 and 43.6. HR-MS (ESI) m/z : Calcd for $\text{C}_{20}\text{H}_{18}\text{N}_4\text{O}_5$ $[\text{M}+\text{Na}]^+$: 417.1175, found: 417.1153.

In silico Studies

Molecular docking study with AChE

We evaluated the possible binding modes of the compounds in the AChE binding site through molecular docking studies. Due to significant conformational changes observed on the peripheral anionic site (PAS)⁶⁰, we selected three representative conformations of AChE following an ensemble docking strategy adopted on a previous study^{32,61} in addition to the structure of human AChE complexed with donepezil⁶² (PDB code 4EY7). The ensemble docking strategy consists in docking the compounds into each representative conformation of the receptor aiming to consider the protein flexibility⁶³⁻⁶⁵. The structures selected were 1ZGC²⁸ (*Torpedo californica*), 2CKM²⁹ (*Torpedo californica*), 1Q84³⁰ (*Mus musculus*) and 4EY7⁶² (*Homo sapiens*). All inhibitors from the four representative conformations of AChE interact with both CAS and PAS. Conserved waters were identified through the superposition of the structures and considered explicitly during the docking experiments (Table 4).

The receptor structures were prepared with Protein Preparation Wizard tool from the Schrödinger Suite 2018-4⁶⁶ and the protonation states of the amino acid residues were predicted using PROPKA with pH = 7. Finally, an optimization of the hydrogen bond network of the protein-ligand complexes were performed to adjust

the orientation of the hydrogen atoms, followed by an energy minimization of the hydrogen atoms.

Table 4. Conserved waters considered in the docking experiments.

Water	1ZGC	1Q84	2CKM	4EY7
Wat1	1468	1708	2062	729
Wat2	1481	1755	2054	737
Wat3	1489	1715	2061	722
Wat4	1531	1735	2035	731

The compounds were designed and prepared with LigPrep from Maestro to set up the isomers, protonation states and tautomers with Epik^{67,68} at pH 7.0 \pm 0.4. We applied torsional constraints to some rotatable bonds to keep the planarity observed for some compounds during the docking experiments. The rotatable bond from the amide group was kept fixed to the *trans* conformation on all compounds.

The ensemble docking experiments were performed with the molecular docking program Glide⁶⁹ from Maestro in the XP precision mode – indicated for highly flexible ligands and to reduce false-positives. All the structures were aligned to the 1ZGC conformation using the *super* tool from Pymol. The receptor grids were centered on the native ligand present in the 1Q84 complex (X: 98.06, Y: 53.14 and Z: 22.06). We also redocked the co-crystallized ligands into their respective AChE conformation and to the non-native structures (*i.e.*, cross-docking) to validate the docking protocol, with all of them successfully predicted within 2.0 Å from the experimentally observed conformation. We selected the ligand pose according to the lowest XP Score among all the four AChE conformations used for the ensemble docking protocol.

ADME Prediction in silico

Based on 2D structural models drawn in ChemDraw professional version 15.0, ADME parameters were predicted in silico by using the QikProp v. 3.5 (Schrödinger).

Biological Evaluation

Anti-cholinesterase Activity Assays

Anticholinesterase activity was determined according to Ellman's method²⁷ modified for 96-well plates as previously described¹⁹. All solutions were prepared in tris-HCl buffer (0.02 M, pH = 7.5) and stock solutions of the test compounds were prepared in DMSO (50 mM). In 96-well plates were added solutions with the inhibitor compound at 30 μM final concentration. The vehicle control (DMSO - final concentration 0.2% v/v for AChE) was used as reference (negative control) and the reagent 5,5'-Dithiobis-2-nitrobenzoic acid (DTNB) was added to electric eel acetylcholinesterase (*EeAChE*) or equine serum butyrylcholinesterase (*EqBuChE*) in presence of bovine serum albumin (BSA). Absorbance was recorded using an

iMark plate reader (Bio-Rad) equipped with a light filter of $\lambda = 415$ nm and this measurement used as a blank reference. After 10 min incubation at room temperature, acetylthiocholine iodide (ACTI) or S-butyrylthiocholine iodide (BCTI) was added and absorbance was recorded after 10 min of incubation at room temperature at $\lambda = 415$ nm for 3 times within 30 sec. Enzyme activity was calculated as a percentage of the mean absorbance values measured for the DMSO-treated control, discounted from the mean blank reference values. Assays were performed in triplicate (for standard deviation calculation). Inhibition values were calculated using the Excel program.

Kinetic Assay

Enzyme kinetics was determined according to Ellman's method²⁷ modified for 96-well plates as previously described^{18,19}. Both enzymes were purchased from Sigma Aldrich. Acetylcholinesterase from *Electrophorus electricus* (electric eel) and Butyrylcholinesterase from equine serum. All solutions were prepared in tris-HCl buffer (0.02 M, pH = 7.5) and the stock solutions of the test compounds were prepared in DMSO (2 mM). In 96-well plates were added 150 μ L inhibitor compound solution of compound **3g** at two different concentrations (2 and 4 μ M) distributed in eight sets of triplicates each. Eight sets of DMSO-treated untreated triplicates (final concentration 0.2% v/v of AChE) were used as negative control. Subsequently, was added 60 μ L of DTNB (Ellman's reagent) to 1.1 mM and 30 μ L of isolate *ee*AChE at 0.20 U/mL in the presence of 1 mg/mL bovine serum albumin (BSA). Absorbance was then recorded using an iMark plate reader (Bio-Rad) equipped with $\lambda = 415$ nm light filter and this measurement used as a blank reference. After 10 min incubation at 25°C, 24 μ L of acetylcholine iodide substrate (ACTI) at eight serially diluted concentrations (factor = 1.3) of 2.75 - 0.44 mM (final concentration: 0.25 - 0.04 mM) were added to the respective wells and the absorbance recorded after incubation for 10 min at 25°C at $\lambda = 415$ nm. The Lineweaver-Burk reciprocal plots were obtained by plotting a $1/\text{velocity}$ versus $1/[\text{substrate}]$ and two different inhibitor concentrations for untreated control. The linear regression of each dataset shows a convergent behavior, in ways the region to where the curves converge determine the type of inhibition. The values of K_i , K_i' (competitive and non-competitive inhibition constants respectively), K_m (Michaelis-Menten constant) and V_{max} (maximum speed) were calculated using Graphpad Prism 7.0 using nonlinear regression models for kinetics. enzymatic - inhibition and enzymatic kinetics - substrate versus velocity.

DPPH Scavenging Activity

The ability of compounds PQM-183 to PQM-190 (**3a-h**) to scavenge DPPH free radicals was evaluated according to the method described by Gontijo 2012⁷⁰. All compounds were evaluated at the concentrations of 200, 100, 50, 25, 12.5, 6.25, 3.13 and 1.56 μ M in ethanol. A 4 mL aliquot of each sample was mixed with 1 mL of DPPH (0.5 mM in ethanol). The solution was vigorously stirred at room temperature and after 30 min the absorbance was measured at 517

nm in a UV-vis spectrophotometer (Shimadzu). A low absorbance value indicates effective free radical scavenging. Each solution was analyzed in triplicate and the mean values were plotted to obtain the EC_{50} against DPPH by linear regression. Antioxidants like ascorbic acid and trolox were used as a standard over the same range of concentrations. The radical-scavenging activity was evaluated as the percentage of inhibition according to the following equation: %inhibition = [(absorbance of control - absorbance of sample)/absorbance of control] \times 100.

PAMPA assay

The model mimicking blood-brain barrier (PAMPA BBB). This assay is based on a two 96-well plates in a "sandwich" type system, where one plate overlaps the other. The upper plate, called the donor compartment, refers to the place where the compounds (tests or controls) are diluted in a buffered medium, which is characterized by the presence of a synthetic membrane of PVDF (polyvinylidene fluoride) impregnated with a lipid solution, forming a barrier through which the compounds migrate through a diffusion process to the lower plate called the receptor^{37,71}. The lipid mixture that impregnates the PVDF filter has a different constitution for the BBB (porcine polar membrane lipid extract in dodecane) and GIT (L- α Soy phosphatidylcholine in dodecane) tests. In a 5 ml glass vial, 1 mg of each compound (test or control) was dissolved in 1 ml of ethanol. Then, 500 μ L of ethanol and 3.5 mL of PBS pH 7.4 were added to this solution. These solutions were filtered (PVDF filter: 0.45 μ M) and set aside. Subsequently, the acceptor 96-well microplate was filled with 180 μ L of a solution of PBS pH 7.4: ethanol (70:30). The donor 96-well plate was coated with 5 μ L of porcine brain lipid in dodecane (20mg lipid/mL, in dodecane). After 5 min, the donor plate received, in triplicate, 180 μ L of the solution containing each compound. Then, the donor plate was carefully placed over the recipient, forming the sandwich-type system, which was left to rest for 2 hr and 45 min at room temperature (\pm 25°C) and humidified. After incubation, the donor plate was removed and the concentration of all the compounds in both the acceptor and the donor wells were determined by the UV plate reader, which was read (SpectraMax 5[®] - Molecular Devices) at the wavelengths previously established for each compound. The blank was prepared in the presence of 180 μ L of PBS solution (pH 7.4): ethanol (70:30) (adapted from Li Di work⁴⁰). The optical density values and data analysis were performed in the same manner as described previously in Lopes' work in 2019⁷².

Permeability studies were performed in the same manner as described previously in Lopes' work in 2019⁷². In the model mimicking intestinal permeability (PAMPA GIT) the lipid used was L- α Soy Phosphatidylcholine in Dodecane. Then, in a 5 mL glass vial, 250 μ L of the freshly prepared solution was homogenized with 4750 μ L PBS (pH 6.6) at 10 μ M. The solution was then filtered (PVDF filter: 0.45 μ M) and reserved. Subsequently, 180 μ L of PBS (pH 7.4): DMSO (95:5) solution was added to the wells of the recipient plate and 5 μ L of soybean L- α -phosphatidylcholine lipid solution (20 mg lipid per mL in dodecane) in the wells of the donor plate. The filter plate was

coupled to the receiver plate and was stirred at 50 rpm for 8 hr at room temperature. The both experiments were performed in triplicate and two different analyses ($n = 2$) were performed in the presence of the control compounds ⁷³.

In vitro studies

Cell Cultures

Monkey kidney epithelial VERO cells (CCL) were routinely grown in Dulbecco's modified Eagle's Medium supplemented with 10% fetal bovine serum, 2 mM L-glutamine, 50 U/mL penicillin and 50 µg/mL streptomycin at 37 °C in a humidified incubator with 5% CO₂. Human neuronal (SH-SY5Y) cells were purchased from the Lombardy and Emilia-Romagna Experimental Zootechnic Institute (Italy). SH-SY5Y cells were routinely grown in Dulbecco's modified Eagle's Medium supplemented with 10% fetal bovine serum, 2 mM L-glutamine, 50 U/mL penicillin and 50 µg/mL streptomycin at 37 °C in a humidified incubator with 5% CO₂. SH-SY5Y cells were differentiated into neuron-like cells with retinoic acid (RA, 10 µM) for 6 days ⁷⁴.

Human monocyte THP-1 cells were purchased from Cell bank Interlab Cell Line Collection (Italy). THP-1 cells were routinely grown in Roswell Park Memorial Institute (RPMI) 1640 Medium with phenol red supplemented with 10% fetal bovine serum, 2 mM L-glutamine, 50 U/mL penicillin and 50 µg/mL streptomycin at 37 °C in a humidified incubator with 5% CO₂. THP-1 cells were differentiated into microglial-like cells with phorbol 12-myristate 13-acetate (PMA, 5 ng/mL) for 24 h at 37°C in 5% CO₂.

Cytotoxicity Assays

Cell viability, in terms of mitochondrial metabolic function, was evaluated by the reduction of 3-(4,5-dimethyl-2-thiazolyl)-2,5-diphenyl-2H-tetrazolium bromide (MTT) to its insoluble formazan, as previously described ⁷⁵. Briefly, neuronal SH-SY5Y cells were seeded in a 96-well plate at 2×10^4 cells/well while epithelial VERO cells at 1×10^4 cells/well. Cell cultures were incubated for 24 h before the treatment with the tested compounds. Subsequently, SH-SY5Y cells were treated for 24 h with different concentrations of the tested compound **3g** (2.5 – 80 µM). While VERO cells were treated for 48 h with different concentrations of the tested compound **3g** (1.4 µM - 1428 µM) at 37 °C in 5% CO₂. Then the treatment medium was replaced with MTT solution (0.5 mg/mL) in Hank's Balanced Salt Solution (HBSS) for 2 h at 37 °C in 5% CO₂. After washing with HBSS, formazan crystals were dissolved in isopropanol. The amount of formazan was measured (570 nm, reference filter 690 nm) using a multilabel plate reader (VICTOR™ X3, PerkinElmer, Waltham, MA, USA) and a Anthos Zenyth 200rt microplate reader (Biochrom, UK). The cytotoxicity of the tested compound was obtained by the following formula: $[(A-B) / A \times 100]$ where A represents the absorbance of untreated cells and B the absorbance of cells treated with different concentrations of the tested compounds. Cytotoxic concentration in 50% of cells was determined by linear regression.

Inflammation and neuronal plasticity assay

The anti-inflammatory activity of the tested compound **3g** was evaluated in microglial THP-1 activated by LPS as previously described ⁷⁶. Briefly, THP-1 cells were seeded in a 6-well plate at 2.5×10^6 cells/well, incubated for 24 h with PMA (5 ng/mL) and subsequently, treated for 24 h with LPS (1 µg/mL) in the presence of compound **3g** (10 µM). The neuronal plasticity of the tested compound **3g** was evaluated in differentiated SH-SY5Y. Cells were seeded in 100 mm dish at 1×10^6 cells/dish, differentiated with RA (10 µM) and subsequently, treated for 24 h with compound **3g** (10 µM). Afterward, cell suspension was pelleted, and RNA was extracted by the PureLink RNA Mini Kit (Life Technologies, Carlsbad, CA, USA) according to the manufacturer's guidelines. A total of 1 µg of RNA were used to synthesize cDNA using the SuperScript VILO MasterMix (Invitrogen, Carlsbad, CA, USA). Quantitative RT-PCR was carried out using SYBR Select Master Mix (Invitrogen), and relative normalized expression was calculated by comparing the cycle threshold (Ct) of the target gene (Inducible nitric oxide synthase, iNOS; Interleukin 1 beta, IL-1β; Prostaglandin-endoperoxide synthase 2, COX-2; Synaptophysin, SYP) to that of the reference genes β-Actin and glyceraldehyde-3-phosphate dehydrogenase protein (GAPDH, Life Technologies). All reactions had three technical replicates, and each condition had three biological replicates. Relative quantification was calculated according to the $\Delta\Delta C_t$ method ($2^{-\Delta\Delta C_t}$) with untreated cells as control. Primer sequences used in this study are listed in **Table 5**.

Table 5. Primer sequences for quantitative RT-PCR.

Gene name	Forward/Reverse	5' to 3' Sequence
iNOS	For	TGAACTACGTCCTGTCCCT
	Rev	CTCTTCTTGGGTCTCCGC
IL-1β	For	TGATGGCTTATTACAGTGGCAATG
	Rev	GTAGTGGTGGTCGGAGATTGC
COX-2	For	CAAATCCTTGCTGTCCACCCAT
	Rev	GTGCACTGTGTTGGAGTGGGTTT
SYP	For	GCAGCGGTGGCAGTGGC
	Rev	GGACGGGGTAAGAGAGGGG
B-Actin	For	GCGAGAAGATGACCCAGATC
	Rev	GGATAGCACAGCTGGATAG
GAPDH	For	GGTCGGAGTCAACGGATTTG
	Rev	GGAAGATGGTGGATGGATTC

In vitro activity against Aβ-aggregates

In order to evaluate the activity of PQM-189 (**3g**) in the aggregation of Aβ₁₋₄₂ peptides, an in vitro assay was performed using the marker thioflavin T (ThT). It is a deep yellow pigment that is widely used to visualize and quantify the presence of misfolded protein aggregates (amyloid plaques) in vivo and in vitro. When connected to a structure rich in β-sheets, thioflavin exhibits an increase in fluorescence and a characteristic red shift of the emission spectrum in the 490 nm range when associated with aggregates (Wall et al., 1999). The fluorescent behavior of ThT may be caused by several factors, which can affect the state charge distribution of the compound when excited,

including the association with rigid and highly ordered amyloid structure, or a specific chemical interaction with another protein (Khurana et al, 2005). This marker was diluted in a glycine-NaOH pH 8.5 solution for immediate reading, in the final concentration of 314 μM .

This protocol was adapted from Benseny Cases et al. (2012)⁷⁷. First, A β_{1-42} peptide (Biointech, Brazil) was dissolved in Milli-Q pH 10, divided into 75 μM aliquots, adjusted to pH 4-5 with HCl solution (2 μL), and stored in -80° C until use.

Before the depolymerization assay, the A β_{1-42} solution was incubated in a dry bath at 37°C for 24 hr. On the day of reading, a dark 96-well plate was used and added of 50 μL A β_{1-42} solution (75 μM), as well as 50 μL ThT, 50 μL of PQM-189 (**3g**), and water to complete up to 300 μL . The compound was tested in 3 doses (75 μM). In FlexStation (American Molecular Equipment Company), single-point reading and polymerization analysis were performed at 37°C with 450 nm excitation wavelength and 490 nm emission wavelength, and then kinetic readings were conducted for 1 hr. The readings were performed every 15 min under the previously described conditions, the interaction was observed every 15 min for 1 hr. The whole process was carried out in a dark environment so as not to interfere with ThT fluorescence. All experiments were carried out in experimental triplicates as well as in three independent experiments. The results were analyzed with the aid of the GraphPad Prism® 9.0 software (San Diego, USA). The results obtained when reading of the endpoint in the FlexStation were subjected to the One-way ANOVA test (Analysis of Variance), followed by the Tukey test. The evaluation data at different times was performed by using two-way ANOVA followed by the Bonferroni test. For all data, values where $p < 0.05$ were considered significant.

In vivo studies Animals

Adult male Wistar rats ($n = 7$ per group) were obtained from the Central Animal Facility of Alfnas Federal University and housed under controlled light (12:12 h light-dark cycle; lights on at 7:00 a.m.) and temperature conditions ($23 \pm 2^\circ\text{C}$) with access to water and food. Except for the night before the experiments when they were submitted to overnight fast (8h). The experiments were performed according to the Brazilian Guidelines for Animal Experimentation defined by the National Council for Animal Experimentation Control. The experimental protocol was approved by the local Research Ethics Committee of Alfnas Federal University (protocol 15/2019).

Experimental design

On the day of the test, the feed was removed, and the adult male Wistar rats received vehicle or **3g** by gavage and then, LPS or saline by intraperitoneal administration. After 2 hr, they were submitted to the open field and the previously weighed pelleted feed was reintroduced. The pattern of food intake was monitored and after

24 hr the adult male rats were euthanized to collect brain structures.

Feeding behavior

Before the test day, the adult male Wistar rats were placed in individual boxes and had free access to water and food. On the day of the test, before receiving treatment, the food was removed for 2 hr. After this feeding restriction, the animals were offered pre-weighed pelleted feed and the pattern of food intake was monitored for 24 hr, by weighing the feed at 2, 4, 6 and 24 hr after its reintroduction⁷⁸.

Open field behavioral test

The aim of this test could verify the locomotor activity in rats to discard the possible nonspecific muscle relaxant or sedative effects. Groups of rats ($n=8$) were treated with vehicle or 1 h before the test. Each rat ($n = 8$ per group) was placed in the center of a circular black-bottomed apparatus (60 cm in diameter and 60 cm high walls) and filmed with a digital video camera for 5 min. The analysis was performed using Ethovision XT 9.0 software (computerized observation system capable to measure of locomotor behavior), where we analyzed the distance traveled by the adult male Wistar rats in the arena and its immobility time⁷⁹.

Statistical analysis

Data were analyzed using the software program GraphPad version 9.0 and expressed as mean \pm standard error of mean (SEM). To compare the effect of LPS and pretreatment with compound **3g** *in vivo*, was used two-way ANOVA, followed by the Bonferroni post-test. In *in vitro* study, was used one-way ANOVA followed by Bonferroni post-test. The level of significance was based on p values less than 0.05 ($p < 0.05$).

Conclusions

Currently, it is very well documented that neuroinflammation plays a central role in both early and late stages of the AD-related neurodegeneration. In this sense, an anti-inflammatory pharmacological approach, coupled to neuroprotection and AChE inhibition could be of clinical relevance in a disease-modifying intervention aiming to effectively control the progression of AD. We reported the discovery of PQM-189 (**3g**), designed as a new multifunctional thalidomide-donepezil hybrid compound, with a unique structural architecture and significant neuroprotective and selective AChE inhibitory properties, aside from anti-neuroinflammatory effects evidenced in different *in vitro* and *in vivo* models. In addition, compound **3g** did not exhibit any significant cytotoxicity in different assays. Besides the ability of inhibiting AChE in a selective and mixed mode, compound **3g** recorded the ability to inhibit iNOS and IL-1 β , two important mediators of AD-related brain inflammation. According to the multiple factors related to the pathogenesis of DNs, compound PQM-189 (**3g**) could represent a

promising drug prototype candidate. This compound is suggested for further studies in drug discovery and development of genuine multi-target directed drugs for NDs therapeutics.

Conflict of interest

The authors declare that there are no conflicts of interest.

Acknowledgments

The authors are grateful to the Brazilian Agencies CNPq (#454088/2014-0, #400271/2014-1, #310082/2016-1, #406739/2018-8 and #303804/2020-3), FAPEMIG (#CEX-APQ-00241-15 and #CEX - APQ-00518-17), FINEP, INCT-INOVAR (#465.249/2014-0), PRPPG-UNIFAL for financial support and fellowships. This study was also financed in part by the Coordenação de Aperfeiçoamento de Pessoal de Nível Superior- Brazil (CAPES) - Finance Code 001.

References

- Businaro, R.; Corsi, M.; Asprino, R.; Di Lorenzo, C.; Laskin, D.; Corbo, R. M.; Ricci, S.; Pinto, A. Modulation of Inflammation as a Way of Delaying Alzheimer's Disease Progression: The Diet's Role. *Curr. Alzheimer Res.* **2018**, *15* (4), 363–380.
- Gelders, G.; Baekelandt, V.; Van der Perren, A. Linking Neuroinflammation and Neurodegeneration in Parkinson's Disease. *J. Immunol. Res.* **2018**, *2018*, 1–12.
- Lois, C.; González, I.; Izquierdo-García, D.; Zürcher, N. R.; Wilkens, P.; Loggia, M. L.; Hooker, J. M.; Rosas, H. D. Neuroinflammation in Huntington's Disease: New Insights with 11C-PBR28 PET/MRI. *ACS Chem. Neurosci.* **2018**, *9* (11), 2563–2571.
- Haase, S.; Linker, R. A. Inflammation in Multiple Sclerosis. *Ther. Adv. Neurol. Disord.* **2021**, *14*.
- Yates, D. Neurodegenerative Disease: A Proteostatic Boost. *Nat. Rev. Neurosci.* **2018**, *19* (2), 61–61.
- Fischer, R.; Maier, O. Interrelation of Oxidative Stress and Inflammation in Neurodegenerative Disease: Role of TNF. *Oxid. Med. Cell. Longev.* **2015**, *2015*, 1–18.
- Schain, M.; Kreisl, W. C. Neuroinflammation in Neurodegenerative Disorders—a Review. *Curr. Neurol. Neurosci. Rep.* **2017**, *17* (3), 25.
- Liu, Z.; Zhou, T.; Ziegler, A. C.; Dimitrion, P.; Zuo, L. Oxidative Stress in Neurodegenerative Diseases: From Molecular Mechanisms to Clinical Applications. *Oxid. Med. Cell. Longev.* **2017**, *2017*, 1–11.
- Cobley, J. N.; Fiorello, M. L.; Bailey, D. M. 13 Reasons Why the Brain Is Susceptible to Oxidative Stress. *Redox Biol.* **2018**, *15*, 490–503.
- Minhas, R.; Bansal, Y.; Bansal, G. Inducible Nitric Oxide Synthase Inhibitors: A Comprehensive Update. *Med. Res. Rev.* **2020**, *40* (3), 823–855.
- Nakamura, T.; Lipton, S. A. Protein S-Nitrosylation as a Therapeutic Target for Neurodegenerative Diseases. *Trends Pharmacol. Sci.* **2016**, *37* (1), 73–84.
- Soufli, I.; Toumi, R.; Rafa, H.; Touil-Boukoffa, C. Overview of Cytokines and Nitric Oxide Involvement in Immuno-Pathogenesis of Inflammatory Bowel Diseases. *World J. Gastrointest. Pharmacol. Ther.* **2016**, *7* (3), 353.
- Kim, M. E.; Na, J. Y.; Park, Y. D.; Lee, J. S. Anti-Neuroinflammatory Effects of Vanillin Through the Regulation of Inflammatory Factors and NF- κ B Signaling in LPS-Stimulated Microglia. *Appl. Biochem. Biotechnol.* **2019**, *187* (3), 884–893.
- Reale, M.; Costantini, E. Cholinergic Modulation of the Immune System in Neuroinflammatory Diseases. *Diseases* **2021**, *9* (2), 29.
- Benfante, R.; Di Lascio, S.; Cardani, S.; Fornasari, D. Acetylcholinesterase Inhibitors Targeting the Cholinergic Anti-Inflammatory Pathway: A New Therapeutic Perspective in Aging-Related Disorders. *Aging Clin. Exp. Res.* **2021**, *33* (4), 823–834.
- de Freitas Silva, M.; Dias, K. S. T.; Gontijo, V. S.; Ortiz, C. J. C.; Viegas, C. Multi-Target Directed Drugs as a Modern Approach for Drug Design Towards Alzheimer's Disease: An Update. *Curr. Med. Chem.* **2018**, *25* (29), 3491–3525.
- Vargesson, N. Thalidomide-induced Teratogenesis: History and Mechanisms. *Birth Defects Res. Part C Embryo Today Rev.* **2015**, *105* (2), 140–156.
- de Souza, G. A.; da Silva, S. J.; Del Cistia, C. de N.; Pitasse-Santos, P.; Pires, L. de O.; Passos, Y. M.; Cordeiro, Y.; Cardoso, C. M.; Castro, R. N.; Sant'Anna, C. M. R.; Kümmerle, A. E. Discovery of Novel Dual-Active 3-(4-(Dimethylamino)Phenyl)-7-Aminoalcoxy-Coumarin as Potent and Selective Acetylcholinesterase Inhibitor and Antioxidant. *J. Enzyme Inhib. Med. Chem.* **2019**, *34* (1), 631–637.
- Santos, S. N.; Alves de Souza, G.; Pereira, T. M.; Franco, D. P.; de Nigris Del Cistia, C.; Sant'Anna, C. M. R.; Lacerda, R. B.; Kümmerle, A. E. Regioselective Microwave Synthesis and Derivatization of 1,5-Diaryl-3-Amino-1,2,4-Triazoles and a Study of Their Cholinesterase Inhibition Properties. *RSC Adv.* **2019**, *9* (35), 20356–20369.
- Kabasakal, L.; Alan, S. Thalidomide Attenuates Learning and Memory Deficits Induced by Intracerebroventricular Administration of Streptozotocin in Rats. *Biotech. Histochem.* **2012**, *88* (3–4), 145–152.
- Palencia, G.; Ángel, J.; Medrano, N.; Ortiz-plata, A.; Jiménez, D.; Sotelo, J.; Sánchez, A.; Trejo-solís, C. Anti-Apoptotic, Anti-Oxidant, and Anti-Inflammatory Effects of Thalidomide on Cerebral Ischemia/Reperfusion Injury in

- Rats. *J. Neurol. Sci.* **2015**, *351* (1–2), 78–87.
- (22) Luzzio, F. A. Thalidomide and Analogues. *Imides Med. Agric. Synth. Appl. Nat. Prod. Chem.* **2019**, 367–429.
- (23) Casal, J. J.; Bollini, M.; Lombardo, M. E.; Bruno, A. M. Thalidomide Analogues: Tumor Necrosis Factor-Alpha Inhibitors and Their Evaluation as Anti-Inflammatory Agents. *Eur. J. Pharm. Sci.* **2016**, *83*, 114–119.
- (24) Silva, V. C.; Giusti-Paiva, A. Sickness Behavior Is Delayed in Hypothyroid Mice. *Brain. Behav. Immun.* **2015**, *45*, 109–117.
- (25) Pham, T. Q.; Berghofer, P.; Liu, X.; Greguric, I.; Dikic, B.; Ballantyne, P.; Mattner, F.; Nguyen, V.; Loc'h, C.; Katsifis, A. Preparation and Biologic Evaluation of a Novel Radiiodinated Benzylpiperazine, 123I-MEL037, for Malignant Melanoma. *J. Nucl. Med.* **2007**, *48* (8), 1348–1356.
- (26) Kamiński, K.; Obniska, J.; Wiklik, B.; Atamanyuk, D. Synthesis and Anticonvulsant Properties of New Acetamide Derivatives of Phthalimide, and Its Saturated Cyclohexane and Norbornene Analogs. *Eur. J. Med. Chem.* **2011**, *46* (9), 4634–4641.
- (27) Ellman, G. L.; Courtney, K. D.; Andres, V.; Featherstone, R. M. A New and Rapid Colorimetric Determination of Acetylcholinesterase Activity. *Biochem. Pharmacol.* **1961**, *7* (2), 88–95.
- (28) Haviv, H.; Wong, D. M.; Greenblatt, H. M.; Carlier, P. R.; Pang, Y. P.; Silman, I.; Sussman, J. L. Crystal Packing Mediates Enantioselective Ligand Recognition at the Peripheral Site of Acetylcholinesterase. *J. Am. Chem. Soc.* **2005**, *127* (31), 11029–11036.
- (29) Rydberg, E. H.; Brumshtein, B.; Greenblatt, H. M.; Wong, D. M.; Shaya, D.; Williams, L. D.; Carlier, P. R.; Pang, Y. P.; Silman, I.; Sussman, J. L. Complexes of Alkylene-Linked Tacrine Dimers with Torpedo Californica Acetylcholinesterase: Binding of Bis(5)-Tacrine Produces a Dramatic Rearrangement in the Active-Site Gorge. *J. Med. Chem.* **2006**, *49* (18), 5491–5500.
- (30) Bourne, Y.; Kolb, H. C.; Radić, Z.; Sharpless, K. B.; Taylor, P.; Marchot, P. Freeze-Frame Inhibitor Captures Acetylcholinesterase in a Unique Conformation. *Proc. Natl. Acad. Sci. U. S. A.* **2004**, *101* (6), 1449–1454.
- (31) Harel, M.; Schalk, I.; Ehret-Sabatier, L.; Bouet, F.; Goeldner, M.; Hirth, C.; Axelsen, P. H.; Silman, I.; Sussman, J. L. Quaternary Ligand Binding to Aromatic Residues in the Active-Site Gorge of Acetylcholinesterase. *Proc. Natl. Acad. Sci. U. S. A.* **1993**, *90* (19), 9031–9035.
- (32) Ceschi, M. A.; da Costa, J. S.; Lopes, J. P. B.; Câmara, V. S.; Campo, L. F.; Borges, A. C. de A.; Gonçalves, C. A. S.; de Souza, D. F.; Konrath, E. L.; Karl, A. L. M.; Guedes, I. A.; Dardenne, L. E. Novel Series of Tacrine-Tianeptine Hybrids: Synthesis, Cholinesterase Inhibitory Activity, S100B Secretion and a Molecular Modeling Approach. *Eur. J. Med. Chem.* **2016**, *121*, 758–772.
- (33) Liu, Z.; Fang, L.; Zhang, H.; Gou, S.; Chen, L. Design, Synthesis and Biological Evaluation of Multifunctional Tacrine-Curcumin Hybrids as New Cholinesterase Inhibitors with Metal Ions-Chelating and Neuroprotective Property. *Bioorg. Med. Chem.* **2017**, *25* (8), 2387–2398.
- (34) Kujawski, J.; Popielarska, H.; Myka, A.; Drabińska, B.; Bernard, M. The Log P Parameter as a Molecular Descriptor in the Computer-Aided Drug Design – an Overview. *Comput. Methods Sci. Technol.* **2012**, *18* (2), 81–88.
- (35) Rourou, S.; Ben Zakkour, M.; Kallel, H. Adaptation of Vero Cells to Suspension Growth for Rabies Virus Production in Different Serum Free Media. *Vaccine* **2019**, *37* (47), 6987–6995.
- (36) Ammerman, N. C.; Beier-Sexton, M.; Azad, A. F. Growth and Maintenance of Vero Cell Lines. *Curr. Protoc. Microbiol.* **2008**, Appendix 4 (1), Appendix 4E.
- (37) Fortuna, A.; Alves, G.; Soares-da-silva, P.; Falcão, A. Optimization of a Parallel Artificial Membrane Permeability Assay for the Fast and Simultaneous Prediction of Human Intestinal Absorption and Plasma Protein Binding of Drug Candidates: Application to Dibenz[b,f]Azepine-5-Carboxamide Derivatives. *J. Pharm. Sci.* **2012**, *101* (2), 530–540.
- (38) Pérez, D. I.; Pistolozzi, M.; Palomo, V.; Redondo, M.; Fortugno, C.; Gil, C.; Felix, G.; Martinez, A.; Bertucci, C. 5-Imino-1,2,4-Thiadiazoles and Quinazolines Derivatives as Glycogen Synthase Kinase 3 β (GSK-3 β) and Phosphodiesterase 7 (PDE7) Inhibitors: Determination of Blood-Brain Barrier Penetration and Binding to Human Serum Albumin. *Eur. J. Pharm. Sci.* **2012**, *45* (5), 677–684.
- (39) Kansy, M.; Senner, F.; Gubernator, K. Physicochemical High Throughput Screening: Parallel Artificial Membrane Permeation Assay in the Description of Passive Absorption Processes. *Journal of Medicinal Chemistry*. American Chemical Society March 26, 1998, pp 1007–1010.
- (40) Di, L.; Kerns, E. H.; Fan, K.; McConnell, O. J.; Carter, G. T. High Throughput Artificial Membrane Permeability Assay for Blood-Brain Barrier. *Eur. J. Med. Chem.* **2003**, *38* (3), 223–232.
- (41) Doty, K. R.; Guillot-Sestier, M.-V.; Town, T. The Role of the Immune System in Neurodegenerative Disorders: Adaptive or Maladaptive? *Brain Res.* **2015**, *1617*, 155–173.
- (42) Kozela, E.; Juknat, A.; Vogel, Z. Modulation of Astrocyte Activity by Cannabidiol, a Nonpsychoactive Cannabinoid. *Int. J. Mol. Sci.* **2017**, *18* (8), 1669.
- (43) Akiyama, H.; Barger, S.; Barnum, S.; et al. Inflammation and Alzheimer's Disease. *Neurobiol. Aging* **2000**, *21* (3), 383–421.
- (44) Bolós, M.; Perea, J. R.; Avila, J. Alzheimer's Disease as an Inflammatory Disease. *Biomol. Concepts* **2017**, *8* (1), 37–43.

- (45) Shi, S.; Wang, Z.; Qiao, Z. The Multifunctional Anti-Inflammatory Drugs Used in the Therapy of Alzheimer's Disease. *Curr. Med. Chem.* **2013**, *20* (20), 2583–2588.
- (46) Glass, C. K.; Saijo, K.; Winner, B.; Marchetto, M. C.; Gage, F. H. Mechanisms Underlying Inflammation in Neurodegeneration. *Cell* **2010**, *140* (6), 918–934.
- (47) Zhang, J.; Rivest, S. Is Survival Possible Without Arachidonate Metabolites in the Brain During Systemic Infection? *Physiology* **2003**, *18* (4), 137–142.
- (48) Oka, T.; Oka, K.; Scammell, T. E.; Lee, C.; Kelly, J. F.; Nantel, F.; Elmquist, J. K.; Saper, C. B. Relationship of EP1-4 Prostaglandin Receptors with Rat Hypothalamic Cell Groups Involved in Lipopolysaccharide Fever Responses. *J. Comp. Neurol.* **2000**, *428* (1), 20–32.
- (49) Rivest, S. How Circulating Cytokines Trigger the Neural Circuits That Control the Hypothalamic-Pituitary-Adrenal Axis. *Psychoneuroendocrinology* **2001**, *26* (8), 761–788.
- (50) Dantzer, R. Cytokine, Sickness Behavior, and Depression. *Immunol. Allergy Clin. North Am.* **2009**, *29* (2), 247–264.
- (51) Norden, D. M.; Trojanowski, P. J.; Villanueva, E.; Navarro, E.; Godbout, J. P. Sequential Activation of Microglia and Astrocyte Cytokine Expression Precedes Increased Iba-1 or GFAP Immunoreactivity Following Systemic Immune Challenge. *Glia* **2016**, *64* (2), 300–316.
- (52) Hart, B. L. Biological Basis of the Behavior of Sick Animals. *Neurosci. Biobehav. Rev.* **1988**, *12* (2), 123–137.
- (53) Kent, S.; Bluthé, R. M.; Kelley, K. W.; Dantzer, R. Sickness Behavior as a New Target for Drug Development. *Trends Pharmacol. Sci.* **1992**, *13* (C), 24–28.
- (54) Schliebs, R.; Arendt, T. The Cholinergic System in Aging and Neuronal Degeneration. *Behav. Brain Res.* **2011**, *221* (2), 555–563.
- (55) Golia, M. T.; Poggini, S.; Alboni, S.; Garofalo, S.; Ciano Albanese, N.; Viglione, A.; Ajmone-Cat, M. A.; St-Pierre, A.; Brunello, N.; Limatola, C.; Branchi, I.; Maggi, L. Interplay between Inflammation and Neural Plasticity: Both Immune Activation and Suppression Impair LTP and BDNF Expression. *Brain. Behav. Immun.* **2019**, *81*, 484–494.
- (56) Sheppard, O.; Coleman, M. P.; Durrant, C. S. Lipopolysaccharide-Induced Neuroinflammation Induces Presynaptic Disruption through a Direct Action on Brain Tissue Involving Microglia-Derived Interleukin 1 Beta. *J. Neuroinflammation* **2019**, *16* (1), 1–13.
- (57) Wang, F.; Wu, Z.; Zha, X.; Cai, Y.; Wu, B.; Jia, X.; Zhu, D. Concurrent Administration of Thyroxine and Donepezil Induces Plastic Changes in the Prefrontal Cortex of Adult Hypothyroid Rats. *Mol. Med. Rep.* **2017**, *16* (3), 3233–3241.
- (58) Vasilopoulou, F.; Rodríguez-Arévalo, S.; Bagán, A.; Escolano, C.; Griñán-Ferré, C.; Pallàs, M. Disease-Modifying Treatment with I2 Imidazoline Receptor Ligand LSL60101 in an Alzheimer's Disease Mouse Model: A Comparative Study with Donepezil. *Br. J. Pharmacol.* **2021**, *178* (15), 3017–3033.
- (59) Singh, A. K.; Rathi, B.; Medvediev, V. V.; Shishkin, O. V.; Bahadur, V.; Singh, T.; Singh, B. K.; Vijayan, N.; Balachandran, V.; Gorobets, N. Y. Functionalized Organic Frameworks Explored as Second Order NLO Agents. *J. Chem. Sci.* **2016**, *128* (2), 297–309.
- (60) Johnson, G.; Moore, S. The Peripheral Anionic Site of Acetylcholinesterase: Structure, Functions and Potential Role in Rational Drug Design. *Curr. Pharm. Des.* **2006**, *12* (2), 217–225.
- (61) Lopes, J. P. B.; Da Costa, J. S.; Ceschi, M. A.; Gonçalves, C. A. S.; Konrath, E. L.; Karl, L. M.; Guedes, I. A.; Dardenne, L. E. Chiral Bistacrine Analogues: Synthesis, Cholinesterase Inhibitory Activity and a Molecular Modeling Approach. *J. Braz. Chem. Soc.* **2017**, *28* (11), 2218–2228.
- (62) Cheung, J.; Rudolph, M. J.; Burshteyn, F.; Cassidy, M. S.; Gary, E. N.; Love, J.; Franklin, M. C.; Height, J. J. Structures of Human Acetylcholinesterase in Complex with Pharmacologically Important Ligands. *J. Med. Chem.* **2012**, *55* (22), 10282–10286.
- (63) Guedes, I. A.; de Magalhães, C. S.; Dardenne, L. E. Receptor-Ligand Molecular Docking. *Biophys. Rev.* **2014**, *6* (1), 75–87.
- (64) Guedes, I. A.; Pereira, F. S. S.; Dardenne, L. E. Empirical Scoring Functions for Structure-Based Virtual Screening: Applications, Critical Aspects, and Challenges. *Front. Pharmacol.* **2018**, *9* (SEP), 1–18.
- (65) Craig, I. R.; Essex, J. W.; Spiegel, K. Ensemble Docking into Multiple Crystallographically Derived Protein Structures: An Evaluation Based on the Statistical Analysis of Enrichments. *J. Chem. Inf. Model.* **2010**, *50* (4), 511–524.
- (66) Madhavi Sastry, G.; Adzhigirey, M.; Day, T.; Annabhimoju, R.; Sherman, W. Protein and Ligand Preparation: Parameters, Protocols, and Influence on Virtual Screening Enrichments. *J. Comput. Aided. Mol. Des.* **2013**, *27* (3), 221–234.
- (67) Greenwood, J. R.; Calkins, D.; Sullivan, A. P.; Shelley, J. C. Towards the Comprehensive, Rapid, and Accurate Prediction of the Favorable Tautomeric States of Drug-like Molecules in Aqueous Solution. *J. Comput. Aided. Mol. Des.* **2010**, *24* (6–7), 591–604.
- (68) Shelley, J. C.; Cholleti, A.; Frye, L. L.; Greenwood, J. R.; Timlin, M. R.; Uchimaya, M. Epik: A Software Program for PK a Prediction and Protonation State Generation for Drug-like Molecules. *J. Comput. Aided. Mol. Des.* **2007**, *21* (12), 681–691.
- (69) Friesner, R. A.; Murphy, R. B.; Repasky, M. P.; Frye, L. L.; Greenwood, J. R.; Halgren, T. A.; Sanschagrin, P. C.; Mainz, D. T. Extra Precision Glide: Docking and Scoring Incorporating a Model of Hydrophobic Enclosure for

- Protein–Ligand Complexes. *J. Med. Chem.* **2006**, *49* (21), 6177–6196.
- (70) Gontijo, V. S.; De Souza, T. C.; Rosa, I. A.; Soares, M. G.; Da Silva, M. A.; Vilegas, W.; Viegas, C.; Dos Santos, M. H. Isolation and Evaluation of the Antioxidant Activity of Phenolic Constituents of the *Garcinia Brasiliensis* Epicarp. *Food Chem.* **2012**, *132* (3), 1230–1235.
- (71) Chen, X.; Murawski, A.; Patel, K.; Crespi, C. L.; Balimane, P. V. A Novel Design of Artificial Membrane for Improving the PAMPA Model. *Pharm. Res.* **2008**, *25* (7), 1511–1520.
- (72) Lopes, J. P. B.; Silva, L.; Ceschi, M. A.; Lütke, D. S.; Zimmer, A. R.; Ruaro, T. C.; Dantas, R. F.; de Salles, C. M. C.; Silva-Jr, F. P.; Senger, M. R.; Barbosa, G.; Lima, L. M.; Guedes, I. A.; Dardenne, L. E. Synthesis of New Lophine–Carbohydrate Hybrids as Cholinesterase Inhibitors: Cytotoxicity Evaluation and Molecular Modeling. *Medchemcomm* **2019**, *10* (12), 2089–2101.
- (73) Zhu, C.; Jiang, L.; Chen, T. M.; Hwang, K. K. A Comparative Study of Artificial Membrane Permeability Assay for High Throughput Profiling of Drug Absorption Potential. *Eur. J. Med. Chem.* **2002**, *37* (5), 399–407.
- (74) Jämsä, A.; Hasslund, K.; Cowburn, R. F.; Bäckström, A.; Vasänge, M. The Retinoic Acid and Brain-Derived Neurotrophic Factor Differentiated SH-SY5Y Cell Line as a Model for Alzheimer’s Disease-like Tau Phosphorylation. *Biochem. Biophys. Res. Commun.* **2004**, *319* (3), 993–1000.
- (75) Pruccoli, L.; Morroni, F.; Sita, G.; Hrelia, P.; Tarozzi, A. Esculetin as a Bifunctional Antioxidant Prevents and Counteracts the Oxidative Stress and Neuronal Death Induced by Amyloid Protein in Sh-Sy5y Cells. *Antioxidants* **2020**, *9* (6), 1–16.
- (76) Di Martino, R. M. C.; Pruccoli, L.; Bisi, A.; Gobbi, S.; Rampa, A.; Martinez, A.; Pérez, C.; Martinez-Gonzalez, L.; Paglione, M.; Di Schiavi, E.; Seghetti, F.; Tarozzi, A.; Belluti, F. Novel Curcumin-Diethyl Fumarate Hybrid as a Dualistic GSK-3 β Inhibitor/Nrf2 Inducer for the Treatment of Parkinson’s Disease. *ACS Chem. Neurosci.* **2020**, *11* (17), 2728–2740.
- (77) Benseny-Cases, N.; Klementieva, O.; Cladera, J. In Vitro Oligomerization and Fibrillogenesis of Amyloid-Beta Peptides. *Subcell. Biochem.* **2012**, *65*, 53–74.
- (78) Rorato, R.; Menezes, A. M.; Giusti-Paiva, A.; De Castro, M.; Antunes-Rodrigues, J.; Elias, L. L. K. Prostaglandin Mediates Endotoxaemia-Induced Hypophagia by Activation of pro-Opiomelanocortin and Corticotrophin-Releasing Factor Neurons in Rats. *Exp. Physiol.* **2009**, *94* (3), 371–379.
- (79) Noldus, L. P. J. J.; Spink, A. J.; Tegelenbosch, R. A. J. EthoVision: A Versatile Video Tracking System for Automation of Behavioral Experiments. *Behav. Res. Methods, Instruments, Comput.* **2001**, *33* (3), 398–414.